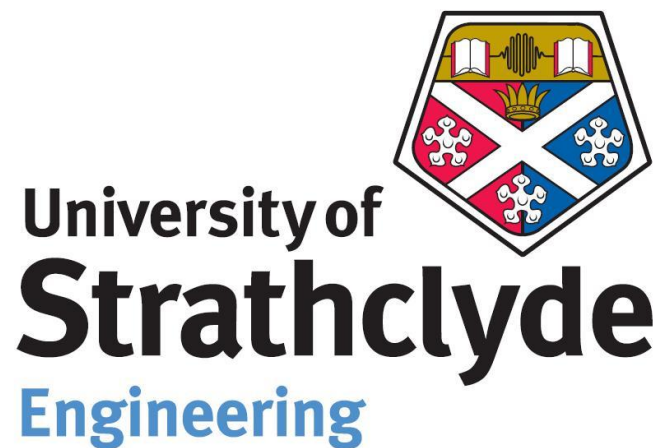


Thesis for the award of Master of Science

**NON-INVASIVE IMPEDANCE MONITORING OF VASCULAR  
CELL GROWTH ON CORONARY STENTS**

Laurent Van Eyck

August 2014



A THESIS SUBMITTED IN PARTIAL FULFILLEMENT OF THE REQUIREMENTS FOR THE DEGREE OF  
MASTER OF SCIENCES IN BIOMEDICAL ENGINEERING

Supervisor:  
Dr. Christopher McCormick.

Department of Biomedical Engineering,  
University of Strathclyde,  
Wolfson Centre,  
106 Rottenrow,  
Glasgow, G4 0NW

## **Author's declaration:**

*This thesis is the result of the author's original research. It has been composed by the author and has not been previously submitted for examination which has led to the award of a degree.*

*The copyright of this thesis belongs to the author under the terms of the United Kingdom Copyright Acts as qualified by University of Strathclyde Regulation 3.50. Due acknowledgement must always be made of the use of any material contained in, or derived from, this thesis.*

*Signed:*

*Date:*

## **Abstract**

Coronary heart disease is the leading cause of death in developed countries. Implantation of a stent, by percutaneous coronary intervention, has emerged as a safe and widely used procedure to address this problem. However, a number of limitations remain with this technique, including potentially delayed healing of the artery endothelium. Recovery of the endothelium is a crucial factor in stent performance and has a strong influence on long term outcomes for the patient. Despite this, the precise mechanisms controlling re-endothelialisation are unclear and there are no means of non-invasively monitoring this process in vivo.

Existing real time monitoring of impedance in cell cultures provides information related to cell activity, adherence and confluence. Therefore, collection of such information applied to coronary stents may be a first step towards a better understanding of their re-endothelialisation. This may also help in understanding the exact duration of antiplatelet therapy required and thus lower treatment costs and improve the long term patient outcomes.

This project investigated the suitability of impedance spectroscopy as a real time technique for monitoring endothelial adhesion and growth on metal surfaces. Primary endothelial cells isolated from freshly excised porcine pulmonary artery were cultured successfully in vitro on a self-manufactured bio-sensor. The cells were also seeded onto a commercially available coronary stent and impedance measurements were made over time. Impedance measurements were performed at different stages of the cell growth in vitro.

It was found that there was a relatively high degree of variability in the impedance measurements obtained. Further analysis revealed that this variability was related to variations in the manufacture process of the biosensors. In a small number of comparable experiments with low variability (n=3), the impedance values collected from the biosensor devices were found to be correlated with cell number. These encouraging findings warrant further investigation of the potential of impedance measurements for monitoring re-endothelialisation of coronary stents in real time.

## **Acknowledgements:**

I would like to express my deepest appreciation to my supervisor, Dr Chris McCormick for offering me this interesting project. I have been extremely lucky to have a supervisor who cared so much about my work, and who allowed me to be curious in my research, I really enjoyed this experience.

I also wish to sincerely thank Ian Holland and Sukhraj Kaloya for their support in the laboratory and for providing support in cell culture.

This thesis would not have been possible without the help, support and patience of the staff, a special thanks to Katie Henderson, John MacLean and Brian Cartlidge for their help on the laboratory and their expertise while teaching me new skills on new devices.

A very big thanks to Dr Mario Giardini for his precious advices, time and sharing his passion in electronics and designs with me. I would like to say a special thanks to my friends Kaushal Khandhar and Vera Hagleitner for supporting me, helping me in writing and being such a nice friends.

I want to thank my family for always supporting me, especially Michel Foucher, Christine & Alain Van Eyck, John & Jimmy Stordeur and Julie Barbagallo.

*To the memory of my dear and honoured father Eric Van Eyck which always inspired me and always supported me in my studies.*

# Table of contents

Author's declaration: .....	II
Abstract: .....	III
Acknowledgements: .....	IV
Table of contents.....	V
List of figures .....	IX
List of tables .....	XII
<b>1. INTRODUCTION .....</b>	<b>- 1 -</b>
1.1. Coronary Artery Disease and treatment.....	- 2 -
1.2. Coronary Artery Bypass Graft (CABG).....	- 3 -
1.3. Percutaneous Coronary Intervention (PCI) .....	- 3 -
1.4. Coronary stenting .....	- 4 -
1.5. Bare-metal stent (BMS) .....	- 5 -
1.6. In Stent Restenosis (ISR).....	- 6 -
1.7. Drug-eluting Stents (DES) .....	- 8 -
1.8. Delayed vessel healing .....	- 9 -
1.9. Late stent thrombosis (LST).....	- 10 -
1.10. Preliminary aim .....	- 12 -
1.11. Impedance spectroscopy .....	- 12 -
1.11.1. Theory.....	- 13 -
1.12. Previous studies.....	- 16 -
1.13. Specific objectives of the study.....	- 19 -

<b>2. METHODOLOGY .....</b>	<b>- 20 -</b>
2.1 Overview .....	- 21 -
2.2. Biosensor chamber development .....	- 21 -
2.2.1 Materials .....	- 21 -
2.2.2. Equipment .....	- 22 -
2.2.3. Methods.....	- 22 -
2.3. Biosensor Characterisation.....	- 25 -
2.3.1. Materials .....	- 25 -
2.3.2. Equipment .....	- 25 -
2.3.3. Methods.....	- 25 -
2.4. Cell Culture.....	- 27 -
2.4.1. Materials .....	- 27 -
2.4.2. Equipment .....	- 28 -
2.4.3. Methods.....	- 28 -
2.5. Impedance Monitoring of cell cultures.....	- 28 -
2.5.1. Materials .....	- 28 -
2.5.2. Equipment .....	- 29 -
2.5.3. Methods.....	- 29 -
2.6. Stent Chamber Pilot Study.....	- 30 -
2.6.1 Materials .....	- 30 -
2.6.1. Equipment .....	- 31 -
2.6.3. Methods.....	- 31 -

<b>3. RESULTS.....</b>	<b>- 34 -</b>
3.1 Overview .....	- 35 -
3.2. Chambers characterisation .....	- 35 -
3.2.1. Leakage test and sterility.....	- 35 -
3.2.2. Impedance measurements in solution A.....	- 36 -
3.2.2.1. Repeatability of impedance measurements .....	- 36 -
3.2.2.2. Variability of impedance measurements .....	- 36 -
3.3. Impedance monitoring of cell cultures.....	- 39 -
3.3.1. Biosensor Microscopy.....	- 46 -
3.4. Stent chamber experiment.....	- 51 -
3.4.1. Stent microscopy.....	- 53 -
<b>4. DISCUSSION.....</b>	<b>- 56 -</b>
4.1. Chapter Overview .....	- 57 -
4.2. Objectives .....	- 57 -
4.2.1. Optimised biosensor chambers development.....	- 57 -
4.2.2. Characterisation of the biosensor chambers .....	- 58 -
4.2.3. Impedance measurements of endothelial cell cultures .....	- 59 -
4.2.4. Stent chamber experiment .....	- 61 -
4.3. Limitations .....	- 62 -
4.4. Future Research .....	- 63 -
4.5. Summary Conclusions .....	- 64 -
<b>5. APPENDIX.....</b>	<b>- 65 -</b>
Appendix A: $ Z $ impedance variability of the control chamber.....	- 66 -

Appendix B: Overheated substrates .....	- 67 -
Appendix C: Future designs.....	- 68 -
<b>6. BIBLIOGRAPHY .....</b>	<b>- 69 -</b>



# List of figures

<b>1. INTRODUCTION.....</b>	<b>- 1 -</b>
Figure 1.1: Illustration of a single, double, triple, and quadruple coronary artery (CABG) bypass.....	- 3 -
Figure 1.2: Main sequence of event occurring in a PCI .....	- 5 -
Figure 1.3: Sectional views of the stented vessel .....	- 6 -
Figure 1.4 : Illustration of a DES releasing anti-proliferative agents .....	- 8 -
Figure 1.5: Simplified equivalent circuit an endothelial in a line configuration.....	- 14 -
Figure 1.6: Illustration of the different types of currents occurring in bio-impedance. ....	- 15 -
Figure 1.7: Example of impedance profile.....	- 16 -
Figure 1.8: Apparatus for bio-impedance measurements .....	- 18 -
<b>2. METHODOLOGY.....</b>	<b>- 20 -</b>
Figure 2.1: Sputter coating in process.....	- 22 -
Figure 2.2: Result of the plasma sputter coater.....	- 23 -
Figure 2.3: Preparation for welding.....	- 23 -
Figure 2.4: Bio sensor chamber picture .....	- 24 -
Figure 2.5: Impedance spectroscopy setup .....	- 30 -

Figure 2.6 :	
Planar configuration of the stent .....	- 31 -
Figure 2.7:	
Configuration of the stent chamber .....	- 32 -
<b>3. RESULTS.....</b>	<b>- 34 -</b>
Figure 3.1:	
Comparison of the intra variability of the 5 chambers .....	- 37 -
Figure 3.2:	
Summary of the  Z  impedance values of the chambers measured in a wide range of frequencies (0Hz to 10 <sup>6</sup> Hz).....	- 38 -
Figure 3.3:	
Summary of the  Z  impedance values of the chamber 14, measured in a focused range of frequencies (500Hz to 5000Hz).....	- 40 -
Figure 3.4:	
Average of  Z  values of the four electrodes from the four biosensor compared with the cell free chamber over the 6 days of incubation.....	- 41 -
Figure 3.5:	
Summary of the  Z  value average of the 4 electrodes from the four biosensor chambers containing cells compared with the cell free chamber over the 6 days of incubation .....	- 42 -
Figure 3.6:	
Averages of the  Z  values of the four biosensor chambers containing endothelial cells 24 hr after seeding , compared with the solution A characterisation. ....	- 43 -
Figure 3.7:	
Average of the  Z  values of the chambers against the estimation of the number of cells for each chamber. ....	- 44 -
Figure 3.8:	
Comparison of the measured  Z  values against the experiment day of the selected electrodes .....	- 45 -
Figure 3.9:	
Relation of the  Z  values and the cell number estimation, between the 3 cell culture chambers from figure 3.7 compared to the cell free chamber. ....	- 46 -
Figure 3.10:	
Endothelial cells cultured within the chamber 10 on electrode E3 .....	- 47 -

Figure 3.11: Endothelial cells cultured within the chamber 11 on electrode E1.....	- 49 -
Figure 3.12: Endothelial cells cultured within the chamber 12 on electrode E2.....	- 50 -
Figure 3.13: Endothelial cells cultured within the chamber 13 on electrode E3.....	- 51 -
Figure 3.14:  Z  impedance values of the electrodes of the stent chamber measured across a wide range of frequencies (1 MHz).....	- 52 -
Figure 3.15:  Z  impedance values of the electrodes of the stent chamber measured at 2 kHz over the 3 days of incubation.....	- 53 -
Figure 3.16: Light microscopy of the struts of the coronary stent on the stent chamber 72h after seeding endothelial cells.....	- 54 -
Figure 3.17: Fluorescence imaging of fixed samples on the struts of the coronary stent...	- 54 -
Figure 3.17: Fluorescence imaging of fixed samples on the struts of the coronary stent . .	- 55 -
<b>5. APPENDIX.....</b>	<b>- 65 -</b>
Figure 5.1: Complete graph of CH14E1 as an example of variability of  Z  impedance values measured in the total range of frequencies across the 6 days with only medium as filled solution. ....	- 66 -
Figure 5.2: Samples of special reliefs observed on different places of the overheated substrate.....	- 67 -
Figure 5.3: Example of possible future design for biosensor masks: Inter-digital sensor array.....	- 68 -

## List of tables

Table 1.1: Different stages of neointima formation following stent implantation .....	- 7 -
Table 3.1: Repeatability of the impedance experiments on solution A within the same electrode with three consecutive tests marked a, b, c .....	- 36 -
Table 3.2: Variability of the measurements with solution A, within the same chamber.	- 36 -

# **1. Introduction**

## 1.1. Coronary Artery Disease and treatment

Coronary heart disease (CHD) or ischemic heart disease is the biggest killer in developed countries. In the United Kingdom, CHD accounts for around 82,000 deaths each year (NHS report, 2012).

The formation of atherosclerosis is the main cause of CHD. It is a complex progressive inflammatory disease which reduces the lumen size of the vessel by an agglomeration and construction of fatty compounds in the arterial walls of the vessel (Lusis, 2000). Importantly, it also makes the walls of the vessel less elastic and calcified.

The heart needs - as any organ in the body - a constant oxygen and nutrition supply carried by the blood. The left and right coronary arteries are the two main vessels responsible for the oxygenation and nutrition of the heart. Within these vessels is where blood pressure is at its highest in the systemic circuit. The heart motion stretches and recoils those arteries depending on contraction and relaxation of the heart (Martini *et al*, 2011). Because these vessels are so crucial and need to be able to expand and contract, atherosclerosis is therefore a significant problem for the patient and hence they are said to have a coronary heart disease (CHD). This disease is also characterised by a reduction in the lumen of a portion of a vessel, commonly termed a stenosis. In this case, the normal blood transport is perturbed or completely blocked and therefore cannot effectively respond to the demand from the surrounding cardiac tissue. This can lead to an ischemia of the local downstream heart tissues. This can lead to a heart attack or hypoxic brain injury and given the seriousness of these risks, it is often necessary to carry out a revascularisation procedure.

Revascularisations can be performed in two main ways:

- Surgery : Coronary Artery Bypass Graft (CABG)
- Minimally invasive procedure : Percutaneous Coronary Intervention (PCI)

## 1.2. Coronary Artery Bypass Graft (CABG)

Around 20,000 CABG procedures are performed in the UK each year with 80% of these cases carried out on patients over 60 years old (NHS Choices, 2014). This is a surgical procedure where the surgeons bypass a blockage in an artery by connecting or grafting a section of another vessel collected from the chest, leg or arm of the patient. Therefore the blood supply is re-established by this new grafted section (see figure 1.1).

CABG is a complex operation performed under general anaesthesia, where the chest is open, the heart is stopped and an extra-corporeal blood circulation setup is required. This can therefore be considered as a highly invasive operation. This technique remains a standard for complex lesions and for patients with numerous affected lesions. For less complex cases or single lesions a PCI is the preferred solution (Mohr *et al.*, 2013).

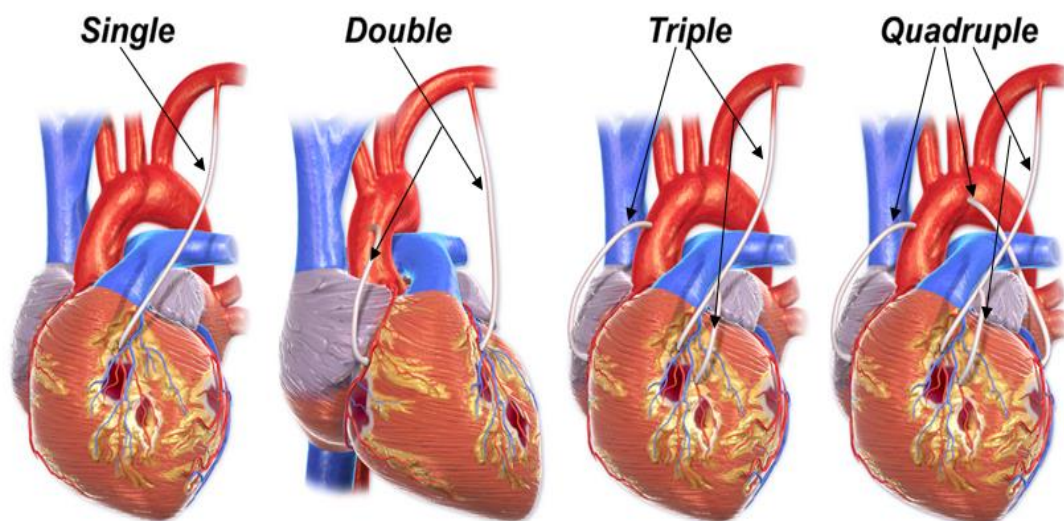


Figure 1.1: Illustration of a single, double, triple, and quadruple coronary artery (CABG) bypass. The arrows show the bypass grafts, providing blood supply from the left subclavian artery and the aorta towards regions affected by atherosclerosis. Blas, 2010.

## 1.3. Percutaneous Coronary Intervention (PCI)

About 75,000 PCI procedures are performed each year in UK and these are mostly on subjects over 65 years old (NHS Choices., 2013). There are consequently about four times more PCI interventions than CABG procedures in

the UK. This procedure is termed as a minimally invasive treatment, in comparison to CABG surgery.

PCI is the combination of a coronary angioplasty followed by stenting. The term angioplasty refers to the procedure where a balloon is used to stretch the narrowed or blocked artery in order to restore a normal blood flow. Stenting of the vessel was added to angioplasty alone to help address serious limitations of the original technique. These limitations include:

1. Abrupt vessel closure: Total shrinking of the lumen of the vessel 0 to 5 days after intervention, which leads to the same effect as a blood clot blockage (Lincoff *et al.*, 1992)
2. Elastic recoil: partial shrinking of luminal area after balloon angioplasty, in other words the lumen returns to its original configuration, as an intrinsic elastic behaviour from the vessel
3. High re-stenosis rates: Repeat narrowing of the vessel occurs for 40% of the cases with balloon angioplasty after around 6 months (Serruys *et al.*, 1994)

## 1.4. Coronary stenting

Stenting is the procedure which aims to restore blood flow, by positioning a stent at the site of the stenosis, which is then expanded against the inner walls of the vessel. A stent is a mesh-like metal device with a tubular shape (figure 1.2F) which has the capacity to expand (figure 1.2D) and keep its last shape after deployment. In PCI, the stent comes after a balloon angioplasty to support the vessel to stay open and prevent future recoil.

A brief summary of the main steps of a PCI intervention is given in figure 1.2. A catheter is first inserted via a guide wire (commonly via the femoral artery) and the cardiologist will inject contrast medium in order to localise and visualise the coronary artery blockage by angiography.



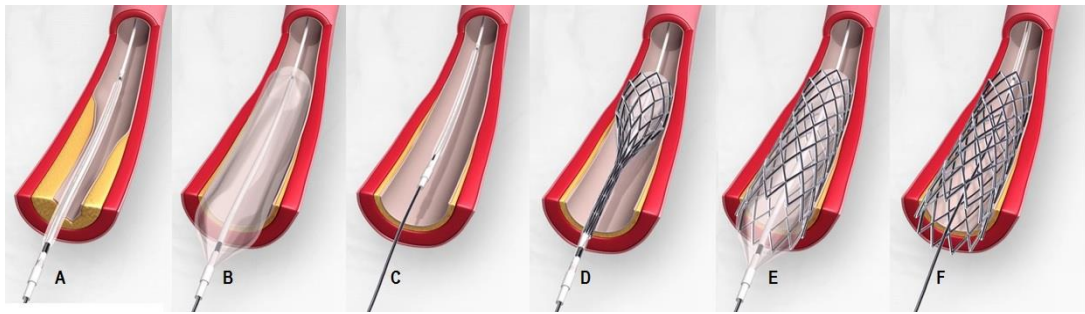


**Figure 1.2:** Main sequence of event occurring in a PCI. The Yellow matter in the image A represent the plaque, or atherosclerosis. B the balloon is inflated. C the plaque is crushed against the artery wall. D. Removal of the deflated balloon. E. The stent is deployed with the balloon inflated in the lumen of the stent. F. The stent is deployed and prevent the plaque to re-tight the vessel diameter such as in image A. American Heart Association, 2014.

Angioplasty then takes place by delivery of the balloon along the guide-wire (figure 1.2A). When the position is confirmed, the balloon is inflated (figure 1.2B) to crush the plaque against the artery wall. After removal of the deflated balloon (figure 1.2C), the stent is deployed at the target place thanks to the pressure balloon inflated in the lumen of the stent (figure 1.2 D&E). The catheter is then removed and only the stent stays at the deployment place (figure 1.2F).

## 1.5. Bare-metal stent (BMS)

Since their first use around 28 years ago, many different generations of stents have been developed, with improved materials, coatings and geometries.

The bare-metal stent (BMS) was the first generation of stent and was commonly made from stainless steel 316L. More recent stents now use cobalt chromium alloys, although stainless steel is still used. In 1986 the first 24 stents for coronary artery were introduced to 19 patients and showed significant improvements in restenosis rates compared to balloon angioplasty (Sigwart *et al.*, 1987).

The main problem with BMS is that the patients who are treated with these devices are likely to suffer from a hyper proliferation of new smooth muscle cells in the tunica intima where the stent is located, following the PCI. This may result in a thickening of the vessel wall (neointimal hyperplasia) through the mesh structure of the stent. This phenomenon is called in-stent restenosis (ISR).

In stent restenosis can occur in 20 to 80 % of the cases with bare metal stents (Kipshidze *et al.*, 2004). This is a very important limitation because ISR is difficult to treat and often requires another stent (revascularisation) or even a CABG operation.

This limitation has driven researchers to develop drug-eluting stents (DES) and details of these will be covered in section 1.6. However, in order to place the use of DES into context, it is important to firstly describe the main mechanisms responsible for the occurrence of ISR.

## 1.6. In Stent Restenosis (ISR)

In-Stent Restenosis (ISR) is the term used to describe the events leading to the recurrence of stenosis in the lumen of the stented vessel. It is characterised by a progressive decrease of the lumen of the stented vessel, which results in at least a 50% reduction in vessel lumen area (Knight *et al.*, 1999).

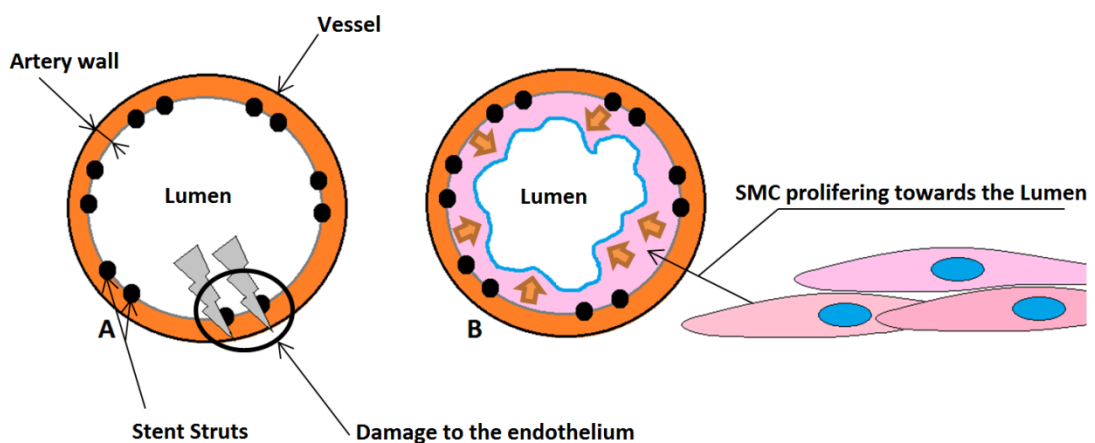


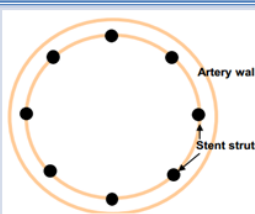
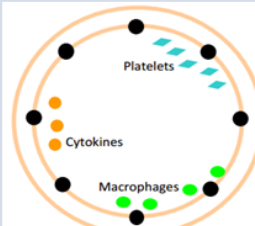
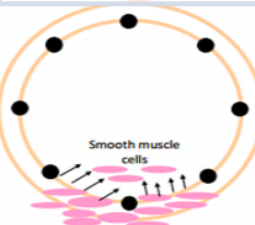
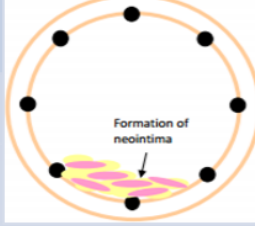
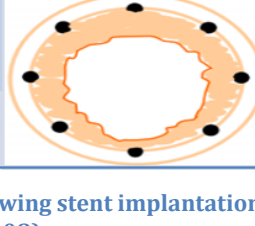
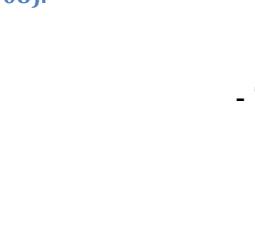

**Figure 1.3: Sectional views of the stented vessel A. Just after stenting, the lumen is wide and kept open by the stent but the stent damage the endothelium of the vessel. B When IRS occurs SMC proliferate towards the centre of the lumen forming with extracellular matrix components, the neo-intima. This reduces the effective sectional area of the blood passage.**

ISR is thought to be originally caused by the severe trauma to the endothelium (Endothelial cell layer) (figure 1.3A) which occurs during the stent placement (Komatsu *et al.*, 1998). The removal of the endothelium, together with the presence of a 'foreign body' within the artery triggers inflammatory responses

involving growth factors which promote neo-intimal hyperplasia (Kirchengast *et al.*, 1998).

It has been shown that the thickness of the neo-intimal tissue formed through the stent (figure 1.3B) is dependent on the depth of the arterial injury (Schwartz *et al.*, 1994). This means that manufacturers have aimed to develop stents which reduce the depth of the injury.

A summary description and schematic of the key stages of ISR between the initial stent placement and the eventual neo-intima formation are shown in Table 1 below.

<b>1) Stent placement</b>			
Endothelial layer removal	Fracture of internal elastic lamina	Damage to the tunica media	
↓			
<b>2) Damage following the stent placement triggers repairs mechanisms</b>			
Platelet aggregation and thrombus formation	release Cytokines and macrophages	Inflammatory process	
↓			
<b>3) Smooth muscle cells migration and proliferation</b>			
Inflammation process involves generation of growth factors that triggers smooth muscle cells proliferation and migration		The Smooth muscle cell attempt to repair the damage and migrate towards the vessel lumen	
↓			
<b>4) Scar tissue forms ( neointimia ) composed with</b>			
Smooth muscle cells		Bulk volume made of extracellular matrix, proteoglycans and collagen	
↓			
<b>5) The neointimia will continue to grow and will tend to provoke the same intitial symptoms that the narrowing with atherosclerosis.</b>			
In stent restenosis is likely to occur in 20 to 80 % of the cases with bare metal stents (Kipshidze <i>et al.</i> , 2004)			

**Table 1.1: Table indicating different stages of neo-intima formation following stent implantation. Images reproduced with the authorization of the author, (Shedden L., 2008).**

Mohan *et alii* conducted a study in 2010 on 80 patients in India, and showed that the restenosis rate was around 48% with bare metal stent treated patients (n= 41) and 13% in those patients treated with drug-eluting stents, (n = 39). Together with earlier studies, such reports confirm that bare metal stents are particularly susceptible to ISR. Patients who develop ISR may need to have a revascularization, which often means a CABG procedure. It is to avoid those cases that the DES were introduced.

## 1.7. Drug-eluting Stents (DES)

Drug-eluting stents were developed after the first generation of BMS to reduce the rates of ISR (Colombo *et al*, 2003; Stone *et al*, 2005.) They achieve this by releasing special drugs (figure 1.4), such as Paclitaxel and Sirolimus, to minimise any further smooth muscle cell proliferation. These drugs are released over a period of weeks by the stent into the vessel walls. They are usually encased within a polymer coating on the stent and this enables a slow release of the drugs into the local tissues over time. The polymers used are an important feature of the performance of the device, as they are in direct contact with the vascular cells and therefore have an important role to play in the biocompatibility of the stent. Mostly because of the special drug releasing features, DES are significantly more expensive than BMS, and the price plays a certain role in the choice of the stent made by the clinician / health provider.

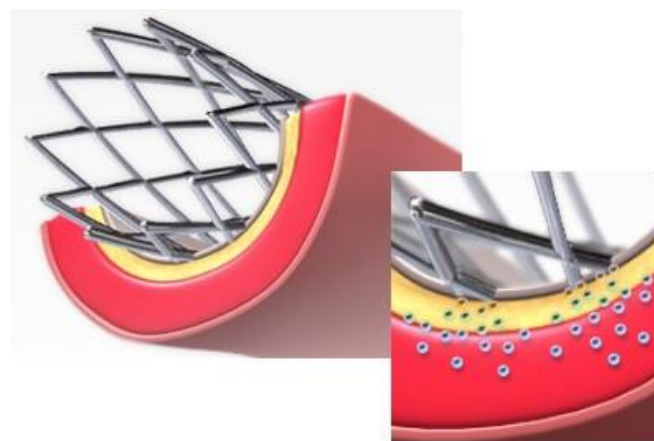


Figure 1.4 : Illustration of a DES releasing anti-proliferative agents (indicated with bubbles) into the inner vessel wall.

American Heart Association, 2014

The drugs reduce neo-intimal formation by disrupting the cell cycle of the smooth muscle cells in order to prevent them proliferating. The two main drugs commonly used, Paclitaxel and Sirolimus, inhibit proliferation but with different mechanisms of action:

Sirolimus (Johnson & Johnson) is a cyto-static agent that causes the cells to arrest without inducing apoptosis. It stops the cell cycle at the G0/G1 phase by acting on the Cyclin-dependent kinase inhibitor 1B (p27Kip1), an enzyme inhibitor which has a crucial role in the regulating the cell cycle (Wessely *et al.*, 2006).

Paclitaxel (Boston Scientific) targets tubulin and cause suppression of spindle microtubule dynamics during the M phase (Mitosis) which prevents the cell proliferation. This drug acts as a mitotic inhibitor (Wessely *et al.*, 2006; Parry *et al.*, 2005).

The most advanced DES have enhanced coatings to encourage better stent endothelialisation (covering of the stent by endothelium layer) including biodegradable polymeric coatings, porous polymer-free coatings (Muramatsu *et al.*, 2013) and bio-resorbable scaffolds (Zhao *et al.*, 2014). However, many of these stents still rely on use of Paclitaxel or Sirolimus and its analogues

Despite the benefits and improvements made with the most recent generations of DES, a certain number of important limitations remain with these devices, such as delayed vessel healing and late stent thrombosis.

## **1.8. Delayed vessel healing**

The role of the endothelium is crucial to maintaining normal vessel function. The endothelium forms a semi-permeable barrier that helps control the exchange of small and large molecules between the circulation and the inner vessel. The endothelial cells (EC), which make up the endothelium, are complex and dynamic cells that are able to perform metabolic and synthetic functions, such as releasing vaso-active substances in response to chemical and physical stimulus (Sumpio *et al.*, 2002). The endothelium plays a central role in a whole

series of processes, including prevention of thrombosis and platelet adherence, regulation of immune and inflammatory responses (including SMC proliferation) and control of blood flow and pressure by adjusting vessel tone (Sumpio *et al.*, 2002). Given that these processes are so important, it is clear that a successful stent must therefore allow complete recovery of this layer.

As we have seen, the drugs used in DES, Sirolimus and Paclitaxel, have anti proliferative effects on smooth muscle cells. However, it has also been shown that this might also inhibit endothelial cell proliferation (Matter *et al* 2006). Given that the endothelium is damaged following the stenting, recovery of the endothelium may therefore be disrupted by these drugs being released into the artery wall. Studies have shown that DES, which release either of these two drugs may have a negative impact on the normal healing process of a damaged arterial wall, which cause delayed re- endothelialisation (Wiskirchen *et al.*, 2004). More recent studies show delayed vessel healing to be multi-factorial phenomenon (Guo *et DiPietro.*, 2010). However, it is still generally accepted that delayed vessel healing after PCI is strongly linked to the incomplete re-endothelialisation and the loss of the endothelial function, leading all together to a risk of late stent thrombosis.

## **1.9. Late stent thrombosis (LST)**

Because the endothelium is not intact immediately following stenting, and the vessel healing may be delayed by the presence of a DES, the vessel is vulnerable to inflammatory process and platelet adhesion, which together contribute to the risk of late or very late thrombosis. (Vodovotz *et al.*, 1999; Salame *et al.*, 2003). Late stent thrombosis is thankfully uncommon (~ 1-2%) (Jaffe *et Strauss.*, 2007). Late stent thrombosis (LST) associated with bare metal stents occurs in around 1-2 % of the cases which is comparable to DES although there remains much debate about this, and some reports suggest a higher rate of late stenosis with DES. (Jaffe *et Strauss.*, 2007). Although relatively rare, LST is a potentially catastrophic event caused by the formation of a blood clot that can cause

dangerous complications including the sudden death of the patient. This risk means that patients need to have dual anti-platelet therapy for a long period of time following DES stent implantation (6- 12 months according the European Society of Cardiology and 12 months for The American College of Cardiology). Importantly, this anti-platelet therapy duration is much longer than is required in BMS patients.

This has led to much research focused on approaches which encourage a more rapid re-endothelialisation following DES procedures. A variety of approaches have been attempted in this pursuit. Certain types of DES coatings aim to attract circulating endothelial progenitor cells in the blood flow to promote in situ regeneration of the endothelium (Ong *et al.*, 2005). Other techniques have been used, such as improving the surface topography of the stent surface because of its critical role in endothelialisation (Mani *et al.*, 2007) or special drugs with anti-oxidant and anti-inflammatory effects, thought to promote re-endothelialisation (Tanous *et al.*, 2006).

Despite these advances, there is currently no technique which is completely effective as a strategy for ensuring a rapid and complete re-endothelialisation, with even the most advanced DES currently used still thought to present a prolonged risk of stent thrombosis. This means that clinicians adopt a conservative approach to minimise the risk of thrombosis. This conservative method tends to deliver the maximum duration time of expensive dual anti-platelet therapy to every patient although not all the patients will have the same recovery rate. Consequently, a certain number of patients will undergo the treatment longer than required. This introduces secondary risks such as an increased risk of bleeding.

Despite the potential benefits of reducing the duration of anti-platelet therapy, the optimal duration for such therapy remains unknown within individual patients (Valgimi *et al.*, 2007). This is mostly due to a lack of reliable information on the time course of stent re-endothelialisation after stenting (Edouard *et al.*, 2003). Better understanding of the re-endothelialisation on

coronary stents is therefore required. However, there is no currently available technique to monitor stent endothelialisation *in vivo*.

## 1.10. Preliminary aim

The overall aim of this study was to investigate methods for real time monitoring of the endothelialisation of coronary stents. This may help to identify when anti-platelet therapy should be stopped. It may also help develop further understanding of the processes governing in-stent endothelialisation *in vivo*.

Whilst there are many potential methods of monitoring cell growth, in the present study we have focused on investigating the potential use of impedance spectroscopy as a non-invasive method of monitoring endothelialisation *in vitro*.

## 1.11. Impedance spectroscopy

As seen previously, re-endothelialisation is a crucial and complex process which is being investigated by researchers in order to improve stent treatment. A real time monitoring of re-endothelialisation may therefore lead to valuable additional knowledge which could be beneficial. For instance, such information may be helpful to manufacturers involved in stent design or it may help inform clinicians who are trying to optimise their patient's anti-platelet therapy regime.

*In vitro* studies have used gold standard techniques such as fluorescent labelling or microscopy (SEM or light microscopy) (Flugelman *et al.*, 1992) to assess endothelial cell adhesion and proliferation. However, these techniques are generally destructive for the cells, making it difficult to monitor re-endothelialisation in real time. Crucially none of those techniques can be readily used *in-vivo*. **Within this context, impedance spectroscopy appears to be a worthwhile option to investigate, since it is non-invasive and can be performed in real time *in vitro* or *in vivo*.** Impedance values can provide valuable qualitative and quantitative information on the degree of cell growth and coverage between electrode pairs (Lind *et al.*, 1991) and we therefore



hypothesised that this technique would be useful for monitoring endothelial cell growth on coronary stent like surfaces.

We will now go on to describe the theory of impedance and outline in more detail its potential role in cell monitoring.

### 1.11.1. Theory

Impedance describes the ability of a material to resist the flow of an electric current through it, without the limitations of Ohm's law which governs only purely resistive compounds on direct currents.

Cells exhibit properties of resistance and capacitance due to the presence of ionic salts and because of the dielectric properties of their phospholipid membranes. These properties can be represented with resistors and capacitors as shown in a simplified example on figure 1.5 which shows a basic cell-electrode-media system. This type of cell impedance characterisation technique has been used widely (Pethig *et al.*, 1987; Rigaud *et al.*, 1996; Valentinuzzi, 1996; Vadim F. Lvovich, 2012).

An electronic circuit comprising of resistors and capacitors in parallel will exhibit typical theoretical response to an increasing frequency sweep. This is explained by the laws which governs the impedance of the capacitive components called capacitive reactance ( $X_c$ ) and given below:

$$X_c = \frac{1}{j\omega C}$$

In the formula below,  $j$  is the imaginary unit,  $w$  is the frequency in rad/sec and  $C$  is capacitance in Farads.

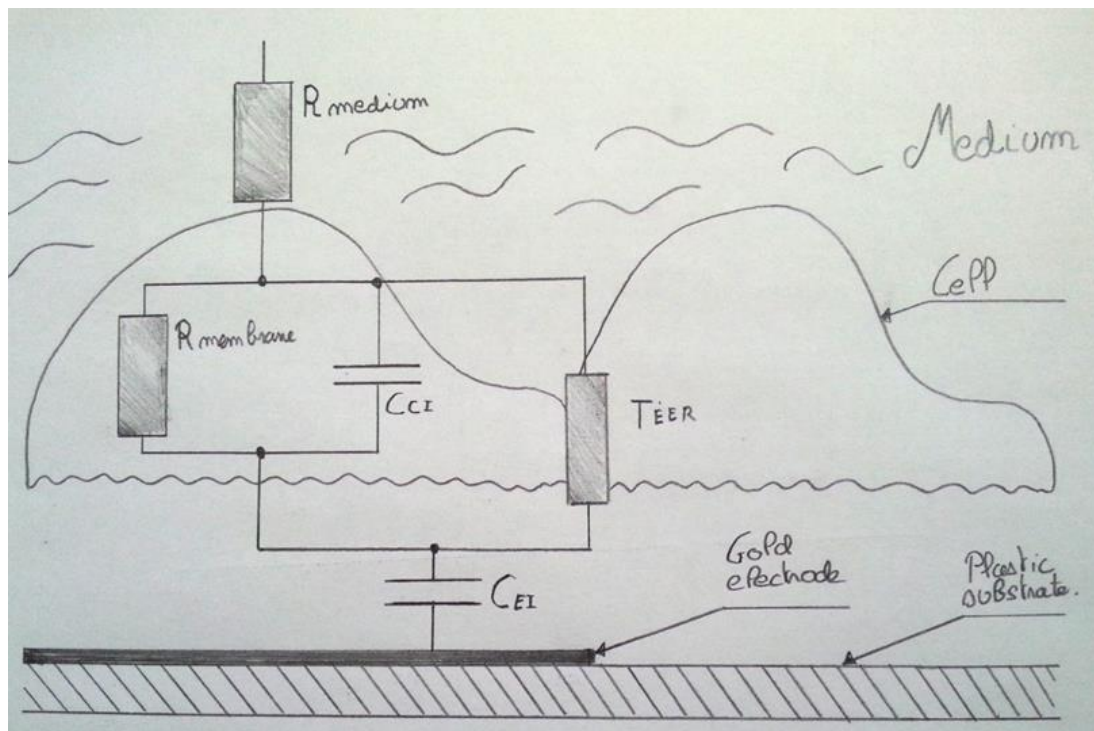


Figure 1.5 shows a Simplified equivalent circuit an endothelial in a line configuration. TEER : the Trans-Endothelial Electric Resistance is the electrical resistance across the cell layer , C1 represent the capacitance or the cell layer , C2 represent the capacitance of the cell - electrode interface ; R2 is the ohmic resistance of the medium and R1 is the ohmic resistance of the cell components. Inspired from Benson *et al*, 2013.

This equation shows that as the frequency ( $\omega$ ) increases, the capacitive reactance value will decrease, which directly affect the path of the current in the circuit (see figure 1.6), as all the resistive components in parallel with capacities will be short-circuited by the reactance. We therefore expect a lower value of total impedance of the cell at high frequencies. In contrast, when the frequency decreases, the values of the reactance rises and the signal gradually has only the choice to pass by the pure resistive components and therefore the total impedance of the cell rises. The consequences of those two behaviours are dependent on the frequency (Valentinuzzi *et al*, 1996) and the current path is not the same, as the current tends to take the easiest route possible. Therefore in lower frequencies, the cells appears to behaves as an insulating spheroid which seems to encourage the current to avoid to pass through the cells (Pethig *et Kell*, 1987) and rather choose to flow around the cells bodies by a path that we will call para-cellular (figure 1.6) in this thesis. The para cellular path can

cross the tight junctions of the cell layer and this resistance is called the TEER (see figure 1.5).

The opposite occurs in higher frequencies as the capacitive components of the cells undergo a decrease in impedance, the current takes a path through the membranes (i.e. trans-cellular path in figure 1.6).

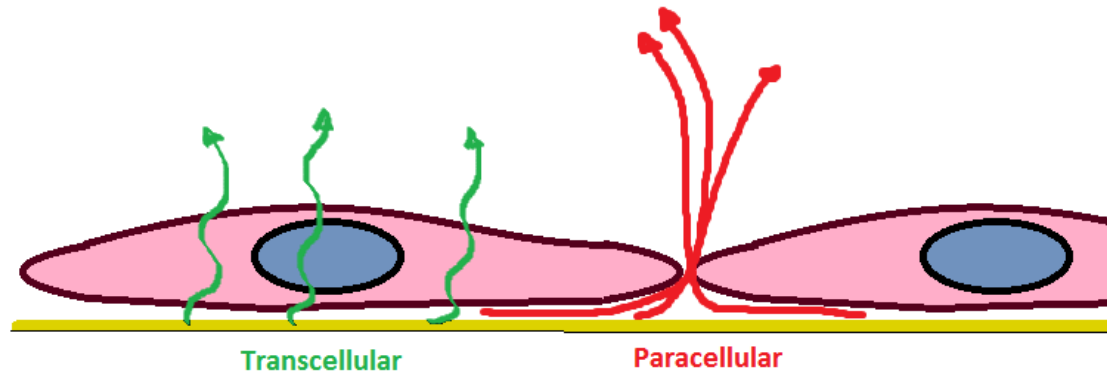


Figure 1.6 shows an illustration of the different types of currents occurring in bio-impedance. In green, the transcellular pathway corresponding to higher frequencies applied. The electric current comes from the gold substrate (yellow base) pass through the cell and passes across the medium towards the reference electrode. When frequency of the signal is lower, the current favours the para-cellular path and flows around the cell.

Except from extreme values ( $f = 0$  or  $f = \text{infinite}$ ) the current path inside the cell is shared between the capacitive and resistive components and is the impedance of those two parts which construct the impedance  $Z$ . This is mathematically represented in a Cartesian form ( $|Z|$ ) and therefore the two components ( $R$  and  $X_c$ ) are represented by respectably real and imaginary numbers.

$$|Z| = \frac{R}{\sqrt{1 + (2\pi fRC)^2}}$$

The formula above shows how the vector  $|Z|$  is worked out as used in Qi Zhong *et alii* work, 2014 who performed a study using a very close setup as what will be used in the present study.

The results of impedance spectroscopy in this study are analysed and compared with computer software, which produces three types of graphs used to characterise the system: A Niquyst plot and two bode plots.

The Impedance ( $|Z|$ ) against frequency show the logarithm of impedance  $|Z|$  as function of the log of the frequency  $f$  (x axis). The behaviour of the  $|Z|$  values over a wide range of frequencies is an impedance signature or impedance profile. An example is given below in the figure 1.7

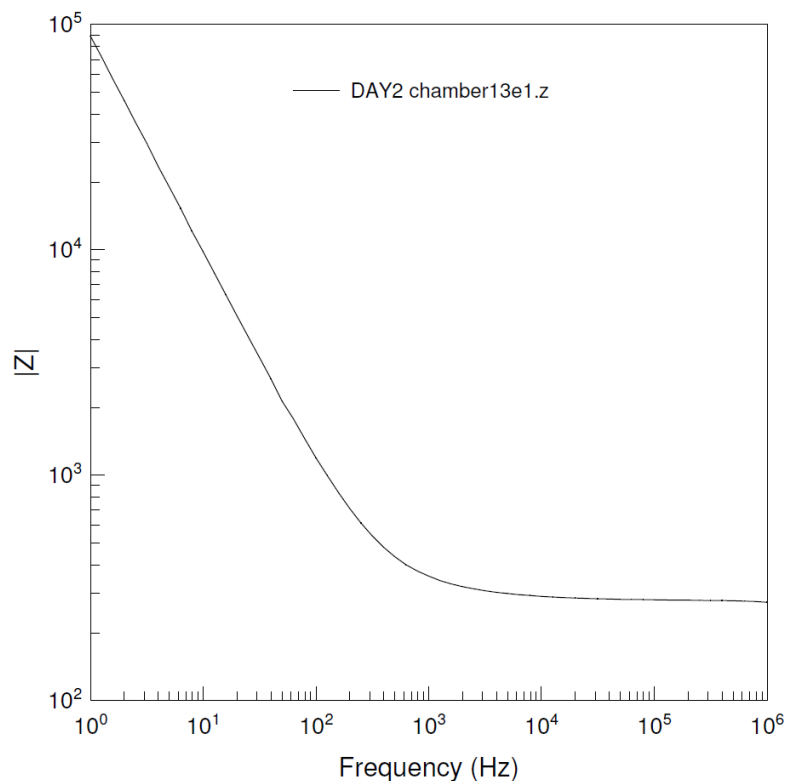


Figure 1.7 shows a bode curve of one impedance profile of the chamber 13, electrode 1 on day 2. As the frequency  $f$  increase the impedance becomes smaller.

## 1.12. Previous studies

The basic principle of using bio-impedance to assess cell culture growth has been demonstrated in numerous previous studies (Beetner *et al.*, 2003; Wegner *et al.*, 1996 & 2000; Zou *et Guo.*, 2003; Shedden *et al.*, 2010) including both *in vivo* and *in vitro* systems.

Studies on various cells involving Electric Cell-Substrate Impedance Sensing (ECIS) have proven that this technique was fully capable of monitoring and assessing the cyto-toxicity, attachment, proliferation, differentiation and death of mammalian cells *in vitro* (Stolwijk *et al.* , 2012 ; Xiao *et al.*, 2008). It has been demonstrated to be a useful tool in cancer diagnostics, such as breast and skin

cancer (Süselbeck *et al.*, 2005) because the measured impedance signal ('signature') is changed due to differences existing between healthy and cancerous tissues (Zou *et Guo.*, 2003). Generally, cancerous tissue has lower impedance over a wide range of frequencies compared to healthy tissues. This is due to macro and micro structural changes in the tissues along with the chemical composition which can be typical to cancerous tissue (Jossinet, J, 1998). Significant differences have also been seen in vitro between healthy and cancerous cells (MCF-10A, MCF-7 and MDA-MB-231). This is shown by a drop in the  $|Z|$  impedance and a corresponding increase in the phase shift.

Within the context of coronary stents, Shedden *et al.*, 2010 reported a method of using impedance to monitor tissue and cell growth around coronary stents. Their study involved a pig coronary artery organ culture model in vitro. They used the bare metal stent (expanded within the coronary artery section) as an electrode in order to measure impedance profiles. The setup is sketched out in figure 1.8. This study emphasised that first of all the presence of the stented artery dominated the circuit in comparison with the control experiment (stent with only media). The complex impedance signal indicated that the biological behaviour of the system was in accordance with the biological Cole equation and tissue presence. An important finding of the study was that the largest changes in the impedance signal, caused by the presence of the tissue, were observed at low frequencies (around 2 kHz).

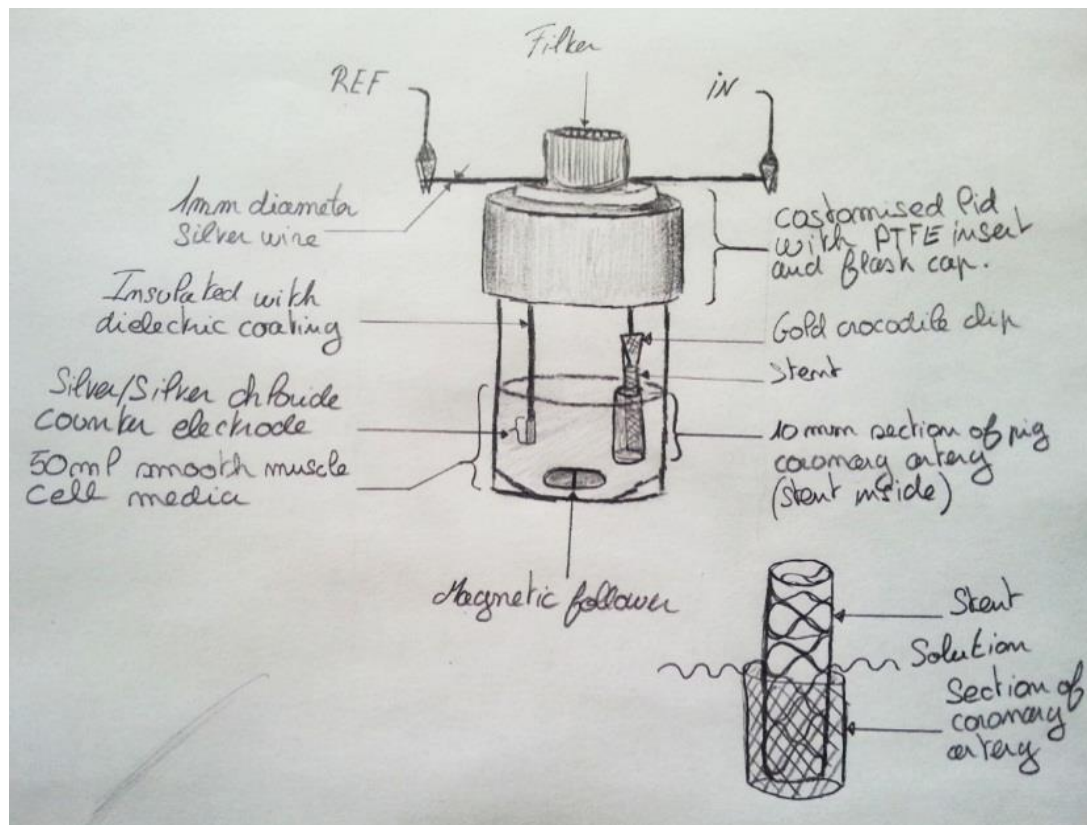


Figure 1.8: Apparatus for bio-impedance measurements, the stent is immersed inside the section of pig coronary artery. Inspired by Shedden *et al.*, 2010.

Shedden's work was the first demonstration of the use of bio-impedance monitoring of tissue growth in situ, in vitro with a coronary stent as an electrode. This high quality work provides a solid basis upon which to proceed in the present study. A weakness of the study was that the experimental set-up used was associated with a high rate of infection of bacteria and fungus, meaning that the n numbers were relatively low. Although the presence of vascular tissue around the stent was successfully monitored using impedance, the specific effect of endothelial cell adhesion to the stent was not investigated in detail. It is therefore important to consider how endothelial cell adhesion has previously been monitored in vitro. An important study in this area was conducted by Wegener *et al* in 2000, which showed that endothelial cell adhesion and proliferation on electrodes gave rise to an increase in the impedance value, Z-modulus (noted  $|Z|$ ).

### **1.13. Specific objectives of the study**

The overall aim of this work was to assess and monitor by impedance measurements endothelial cell growth on metal materials over time.

It was hypothesised that impedance measurements on metals substrates will correlate with the degree of confluence of cells on them.

In theory, the impedance profile impedance should rise in relation to the number of endothelial cells adherent within the cell chambers.

The specific objectives set out in order to achieve this overall aim and test this hypothesis were as follows:

- Develop an optimised cell culture biosensor chamber for recording bio-impedance measurements
- Characterise the repeatability and variability in the biosensor chambers manufacturing process.
- Use the optimised chambers to measure the impedance profiles of endothelial cell cultures at varying points in their growth cycle
- Develop and characterise a modified chamber in order to record impedance on a coronary stent in the presence of endothelial cells.

## 2. Methodology



## 2.1 Overview

Chapter one highlighted the potential of impedance spectroscopy as a minimally-invasive method of monitoring stent endothelialisation.

This chapter aims to provide a full description the experiments methods used to investigate this potential. Details of the biosensor chamber manufacture, endothelial cell culture, impedance spectroscopy and microscopy will all be provided.

## 2.2. Biosensor chamber development

In this study we developed five biosensor chambers in order to measure endothelial cell growth. A greater number of chambers were produced during a preliminary study, during which the methods and materials were optimised. The methods and materials described below represent the results of this early work and relate to the final 5 biosensor chambers, which were used in the study.

### 2.2.1 Materials

Each individual chamber comprised a Falcon™ petri dish (60 x 15 mm Easy-Grip) with standard surface growth polystyrene. In this thesis the culture cubes refers to the small area where the cells are grown. It is performed with Lab Tek chamber slides (model 177429, Nunc) which are attached to the petri dish. These culture cubes were attached with double sided biocompatible tape (Toupee tape, MH Direct, UK). A 1 mm thick metal mask was used in the electrode deposition process (University of Strathclyde, UK). The cold welding of electrodes to connecting wires was carried out with a silver 3G conductive adhesive paint (RS Components Ltd., UK).

## 2.2.2. Equipment

A Biorad SEM Gold coater unit E5175 was used to deposit the gold electrodes onto the surface of the biosensor chambers.

## 2.2.3. Methods

During the whole process we aimed to have the highest repeatability of manufacturing for the apparatus in order to enable effective future comparisons to be made between the results from different chambers.

Holes were first made on the longitudinal axis of a petri dish with a manual drill (5 mm diameter). A manual drill was used in order to increase precision and reduce risks of material rupture. The inner surface of the petri dish was protected using a plastic disk to avoid unwanted material deposition due to human touch or artefacts from the drilling process.

Thereafter, a plasma sputter coating deposition of gold was performed in order to produce the electrode array. This process has been used extensively within the laboratory previously for gold coating of a variety of materials and is based on a well-established methodology (Allen *et* Simmens., 1976). A very short explanation of this process given below:

The gold surface (cathode) is bombarded with accelerated ions, generated by a high voltage potential (1 kV with current limited to less than 30 mA). This produces atomic sized gold particles, which are ejected from the surface of the cathode and are then deposit on the cell culture petri dish immediately below (see figure 2.1) This process takes place in a sealed environment under a partial

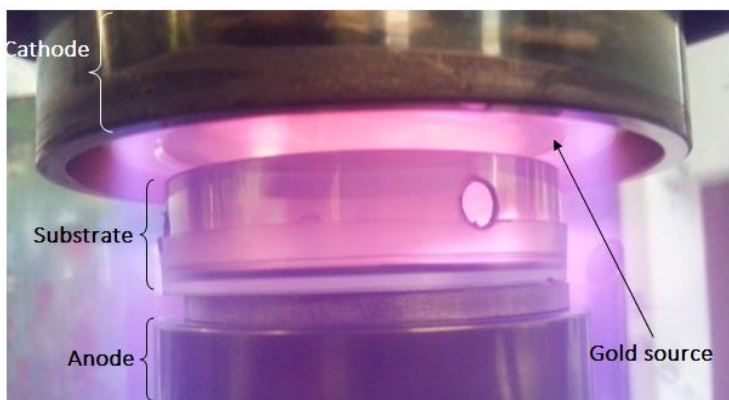


**Figure 2.1: Sputter coating in process.** The substrate is the petri-dish, which is exposed to the glow discharge (plasma) which is visible (cloudy purple beam). This purple beam results from the passage of the accelerated ions from the anode to the cathode through argon gas.

vacuum (0.2 Torr) in the presence of argon gas. The use of a metal mask, shown in figure 2.2, positioned over the cell culture surface of the petri dish during this deposition process, results in an array of gold electrodes being deposited on each plate (figure 2.3, right hand side). It was found that an even distribution of gold electrodes of suitable thickness was produced after four repeat cycles of the above deposition process, with each cycle lasting 30 seconds. Between each cycle, the chamber was allowed to cool in order to prevent melting of the plastic cell culture petri dish.

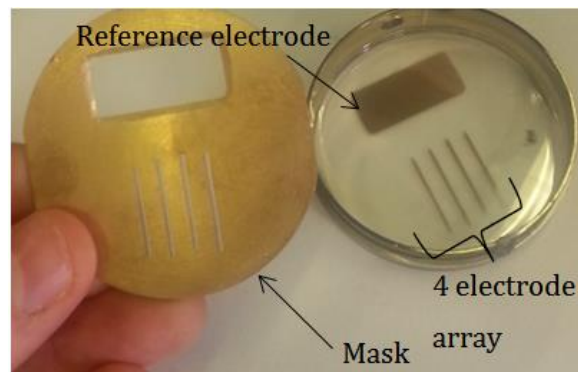


**Figure 2.2:** Result of the plasma sputter coater, the mask allows the exposition of an electrode array of 4 electrodes and one reference electrode.

Following deposition of the electrode array, electrical connections were made to each gold electrode. This was carried out as follows: 7cm copper wires were welded to the electrodes using contact adhesive glue. It was found that gluing the wires inside the chamber before welding allowed a better connection (figure 2.3 left). Each copper wire was then passed through the previously made holes

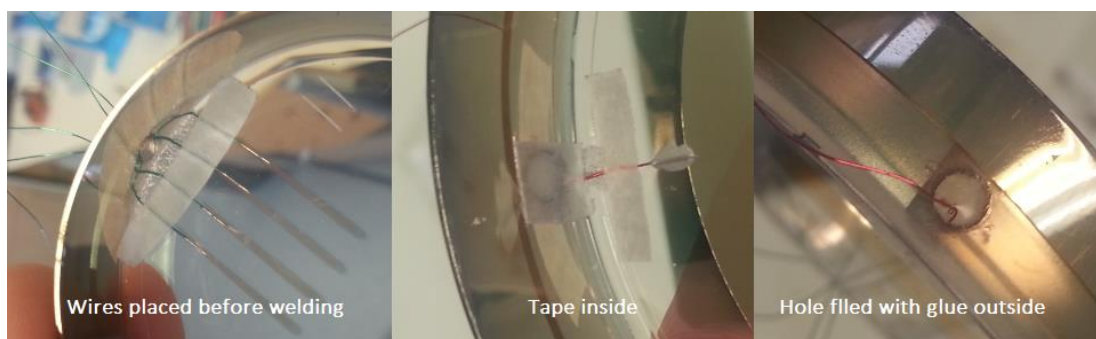


**Figure 2.3:** Shows the preparation for welding. In the right picture the wires are placed against the gold layer thanks to the glue and the stripe of tape previously arranged. The central picture shows the blockage of the one hole from inside the plate, where the connecting wire is passing. This is performed with mask tape in order to prevent any contamination from outside the chamber. On the right, the hole is then filled with glue to solidify the blockage.

in the petri dish, with glue being used to then block the holes to reduce the risk of infection during subsequent cell culture (see figure 2.3 centre and right images)

Thereafter, the square culture cube was placed in the middle of the chamber (see figure 2.4). The culture cube was used as an inner chamber within which the endothelial cells would be grown. It provides a further barrier to infection, and can be easily removed to allow the full culture area to be imaged with a range of microscopy methods. The double Labtek culture slide was cut in a half so that a single square chamber would fit inside the petri-dish. The Permanox slide was carefully removed from the square chamber and it was then attached to the culture dish via double-side tape. It was then compressed with a weight for one night to ensure a secure connection to the underlying petri dish was achieved. This final device is referred to in this study as a biosensor chamber. A schematic description of the device is provided in the figure 2.4. In total, five biosensor chambers were produced using the above method. These will be referred to as: CH 10 – CH 14 through the remainder of this document.

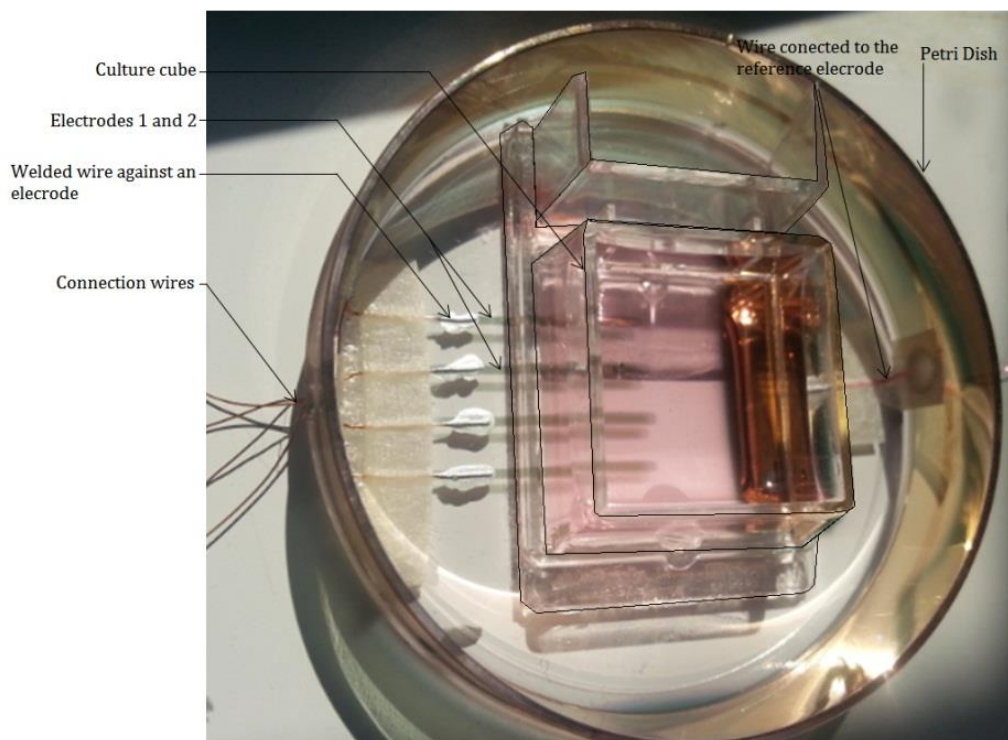


**Figure 2.4:** Description of one bio sensor chamber, the diameter of the petri-dish is 52 mm and the growth area of the cell culture cube is 40mm<sup>2</sup>. In this picture the culture cube contains coloured medium. A plan of the biosensor chamber is given in figure 3.10 panel E.

## 2.3. Biosensor Characterisation

This section of the methodology set out to provide information on the performance of the manufactured chambers prior to cell culture. To do this we first performed a leakage test, followed by impedance measurements with Solution A, a test solution commonly used for such purposes.

### 2.3.1. Materials

The solution A was made of 8.298g of sodium chloride (Sigma-Aldrich, UK) and 0.368g of calcium chloride (anhydrate) (Sigma-Aldrich, UK) mixed in one litre of distilled water.

### 2.3.2. Equipment

Solution A components were weighed with a common laboratory precision balance and mixed with a common vortex stirrer. The impedance measurements were performed with a Solatron model 1260 Impedance/Gain-phase Analyser (Solartron Analytical, Hampshire, UK) and the data processed and recorded with Zplot™ and Zview™ software (Alvatek Ltd, Uk).

### 2.3.3. Methods

#### Leakage test

In order to prevent possible leakages of the medium from the cell culture biosensor chambers, a first leakage test was carried out in each chamber by adding 2ml of distilled water into the culture cube and then monitoring closely for three hours to examine possible leakages. This was carried out at room temperature. In the event of a leakage being observed in a chamber, it was discarded or repaired and retested. All of the chambers used in the endothelial cell monitoring experiments were tested in this way and no leaks were found.

A single chamber was also tested by incubating the chamber containing the distilled water in the cell incubator, in order to mimic the conditions of the final experiment. No leaks or reduction in liquid volume were observed during this test.

### Impedance Measurements in Solution A.

The solution A characterisation was performed to test the biosensor chambers prior to cell seeding and to gauge the capability of the biosensor chambers to record small impedance changes. One litre of solution A was made following a procedure previously used in the laboratory. Briefly, 8.298g of sodium chloride and 0.368g of calcium chloride anhydrate were dissolved in one litre of distilled water. Solution A was stored at room temperature in a glass bottle to help ensure that its temperature was consistent between experiments. Given that it was anticipated that the presence of cells and proteins would alter the impedance measurements between each electrode-reference pairs, it was important to characterise the baseline difference between the chambers independently of these effects. In order to do this, the impedance of each electrode pair within each chamber was measured with the impedance analyser connected to the electrode pair in the presence of solution A. In total 60 impedance measurements with solution A were performed. These involved 3 repeat tests (A - B - C) per electrode for every electrode pairs (E1 - E4), for each chamber (CH10-CH14). One electrode pair represents the combination of one of the small electrodes (E1-4) and the larger reference electrode. The biosensor chambers were characterised according to the repeatability and variability of the impedance measurements obtained:

- **Repeatability:** These were performed in order to understand how precise the recordings from the electrodes were. 3 consecutive impedance measurements were performed on the same electrode for each electrode. We then compared the results to assess the repeatability of the measurements.
- **Variability in impedance measurements:** These tests were carried out to understand the variability in the starting impedance level of each electrode pair between the chambers. The impedance of each electrode of each chamber was recorded and then we compared the values

obtained at different frequencies between the electrodes of the same chamber.

Prior to each measurement, the performance of the impedance analyser was checked with a model parallel RC circuit ( $100\text{k}\Omega/49\mu\text{F}$ ). No differences in the baseline operation of the impedance analyser were observed from day to day.

In all cases reported in this study, the impedance measurements were performed using the following conditions:

Type of measurement: Frequency sweep

Voltage: 10mV

Frequency sweep range: 1Hz - 1MHz

Duration for one Experiment: 61s

Sampling frequency = 1Hz

## **2.4. Cell Culture**

### **2.4.1. Materials**

All materials detailed here were purchased from Life technologies, Glasgow, UK. Cell medium for large vessel endothelial cell culture systems (medium 200™) was supplemented with 2% low serum growth supplement and 1% penicillin-streptomycin. TrypLE™ Express Enzyme (1X) was used in passaging of the cells.

The cells used in the study were primary endothelial cells of passage 3-7. These were made available to the present study by another student working in the laboratory, Sukhraj Kaloya, who had isolated the cells from freshly excised porcine pulmonary artery and cultured them according to methods previously used in the laboratory (McCormick, 2008). Briefly, the cells are obtained by using a scalpel blade to gently scrape a  $9\text{cm}^2$  area of the luminal surface of the pig pulmonary artery to remove the endothelial cells. These cells were then immediately transferred to growth medium and grown in T-25 culture flasks under standard cell culture conditions (37 C, humidified atmosphere containing 5% CO<sub>2</sub>).

Cells were passaged at approximately 70% confluence and media was refreshed every 2-3 days.

### **2.4.2. Equipment**

A MSE mistral 2000 bench top centrifuge was used in the cell seeding preparation. All cell culture work was carried out within a sterile laminar flow workstation (Bassaire Ltd, UK).

### **2.4.3. Methods**

Prior to seeding the endothelial cells into the chambers (CH10-13), each chamber was rinsed in 100% ethanol and allowed to dry in the sterile cell culture workstation. UV light was then switched on for a period of 3 hr to help maximise the sterility of the chambers.

For endothelial cell monitoring experiments, the endothelial cells were seeded to achieve a confluence of approximately 50% in each chamber. A total of 2ml of cell culture medium was added to each chamber and the cells were transferred to the cell culture incubator.

## **2.5. Impedance Monitoring of cell cultures**

As the overall aim of this study was to assess and monitor by impedance measurements EC growth on metal materials over time, the biosensor chambers containing the endothelial cells were observed using microscopy and their impedance recorded at various time points as detailed below.

### **2.5.1. Materials**

The materials and methods used for cell culture are described in the previous section. Phosphate buffered saline solution pH 7.4, Acridine Orange staining solution and Formalin solution were all purchased from Sigma-Aldrich (Poole, UK).



## 2.5.2. Equipment

The Impedance measurements were performed with a Solartron model 1260 Impedance/Gain-phase Analyser (Solartron Analytical, Hampshire, UK) and the data processed and recorded with Zplot™ and Zview™ software (Alvatek Ltd, UK). During the impedance measurements, the biosensor chambers containing the cells are removed from the chamber for periods up to around 15 min. For this reason, a heat mattress was used to maintain the temperature of the chamber at around 37 C during these measurements.

Light microscopy was performed using a Motic AE 34 inverted microscope.

## 2.5.3. Methods

Chamber 10, 11, 12, 13 were seeded as described in the previous section with endothelial cells at day 0. Impedance measurements were performed according to the method described in section 2.3.3 (Impedance measurements in Solution A)

In total, 80 bio-impedance measurements ( $|Z|$  vs. frequency) were performed on these chambers, comprising: 1 measurement for each electrode pair (E1 – E4) for each chamber (CH10-CH14), once a day on Day 1, Day 2, Day 3 and day 6.

The biosensor chamber without cells (control chamber) was chamber 14. The medium in all five chambers was changed once after the impedance measurements on day 3. Following the impedance measurements, light microscopy images were systematically taken from each electrode of each chamber on each day of the experiment. At the end of the experiment on day 6, the cells were lifted from the plate using TrypLE solution and re-suspended in fresh culture media to allow cell counting. The cell number was counted by using a haemocytometer, according to a standard procedure used in laboratory.

Two samples were used for each chamber and the average was calculated in order to provide the cell number per chamber.

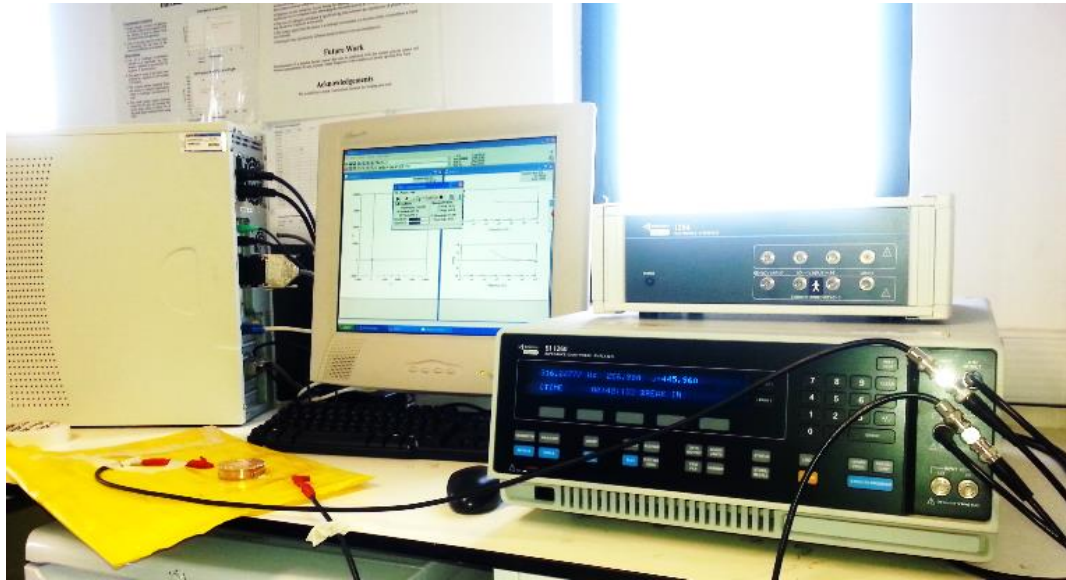


Figure 2.5: impedance spectroscopy setup during the impedance monitoring of cell cultures. This shows the bio impedance recording of an electrode pair. The yellow heat mat is below the biosensor chamber and is set to keep the cells inside the biosensor chamber at 37°C.

## 2.6. Stent Chamber Pilot Study

Since one of the central aims of the present study was to examine the potential of bio-impedance as a method for monitoring endothelial cell growth on coronary stents, it was decided to modify the bio sensor chamber design to allow incorporation of clinically available coronary stent.

Endothelial cells were seeded into a chamber containing one coronary stent and impedance measurements and microscopy were performed daily for three days. The materials and methods used are identical to those previously reported in previous sections except where indicated below.

### 2.6.1 Materials

A stainless steel wire electrode (SS316L, 1mm diameter, Goodfellow, UK) was used as a reference electrode and the coronary stent used was a bare metal

stent, 2.75 x 11mm Gazelle™, Lot W10010025, ref GAZ-2711, (Biosensor International, Singapore, expiry date December 2012).

A large petri dish (Falcon™ petri dish (90 x 25 mm Easy-Grip), a Labteck chamber slide™ (model 177429) and Double-sided biocompatible tape (Toupee tape, MH Direct, UK) and basic strain gauges wires were used to construct the test device (see the two figures in section 2.6.3).

### 2.6.1. Equipment

Light microscopy was performed using a Motic AE 34 inverted microscope and the fluorescence images were captured using a Carl Zeiss Axioimager microscope (Germany), along with Axiovision software.

### 2.6.3. Methods

Cells were seeded on day 0 at the same time and the same degree of confluence and with the same conditions as those used in the biosensor chamber experiments.

A special apparatus (figure 2.7) was designed using broadly the same principles and methods as set out with the same methodology as the biosensor chambers. A planar configuration for the coronary stent was chosen to provide a higher surface area for contact with the cells, and to ensure that the stent was closely

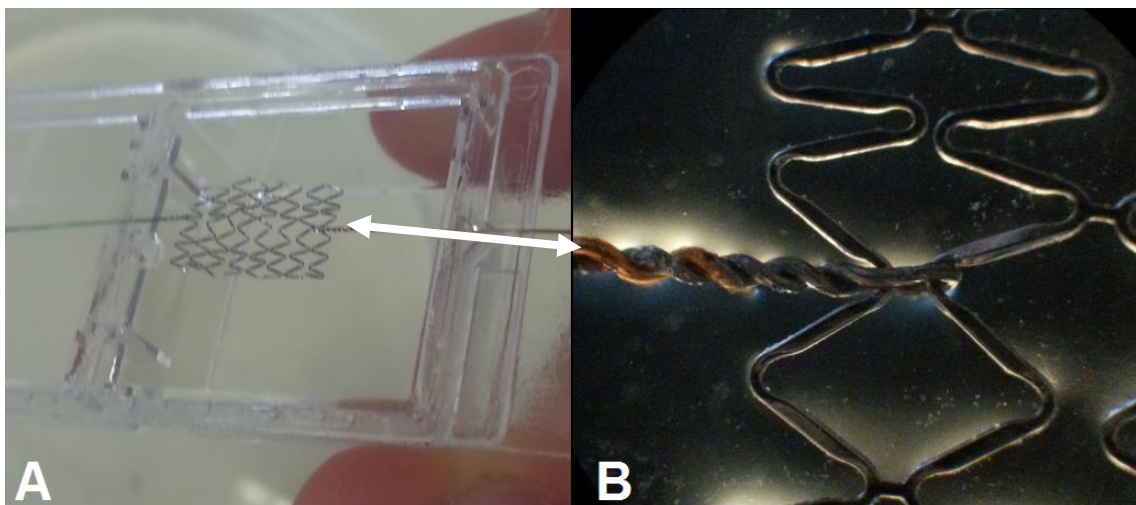
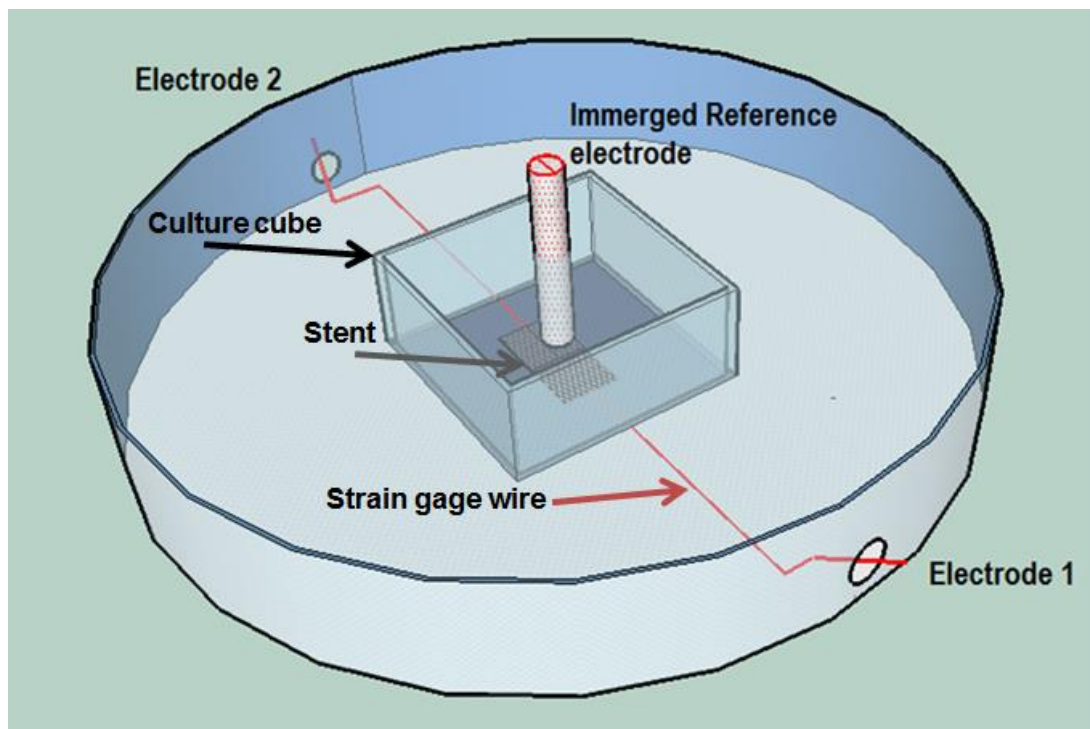


Figure 2.6: A Planar configuration of the stent, the stent is used as the electrode and is mechanically attached with the connecting wires. B attachment of the strain gauges wires to the stent. The double arrow shows the same attachment at different magnifications.

aligned to the bottom of the cell culture chamber. The stent was therefore cut in the longitudinal axis with precision scissors under a light microscope and unfolded into a flat configuration (figure 2.6A). Two strain gauge wires were then attached to the two ends of the stents to enable subsequent impedance measurements to be made (figure 2.6B).

A culture cube was secured around the stent to house the cell culture area. A stainless steel wire electrode (SS316L, 1mm diameter, Goodfellow, UK) was then immersed in the medium by placing it through the culture plate lid. This electrode acts as the reference electrode, thus completing a circuit with the stent acting as the working electrode.



**Figure 2.7: Configuration of the stent chamber. The reference electrode (stainless steel) is passing through the lid and is immersed in the media in the culture cube. See figure 2.6B for electrodes attachment.**

Impedance measurements were made between the following electrodes:

E1 – Reference

E2 – Reference

E1 - E2

In order to qualitatively assess the cell adhesion in terms of confluence, fluorescence imaging was performed. To do this, the stent was gently removed from the chamber and rinsed with PBS solution two times. Formalin was added for 24 hours at 5°C. The stent was then placed in a cell culture dish and given three PBS washes. It was then immersed for about 30 seconds in acridine orange staining solution in total darkness. Following removal of the acridine orange, the stent was rinsed three times and finally immersed in PBS.

The imaging was carried out directly after this using the Zeiss microscope and its user software according to the standard procedure from the laboratory.

## 3. Results

## **3.1 Overview**

The study aimed to monitor the impedance of endothelial cell cultures over time. EC were added to 4 separate biosensor chambers (CH10 - 13) and their impedance profiles were measured at different times over a 6 day period. A cell free chamber (CH14) was used as a control.

In order to assess the quality of the impedance measurements, leakage tests were performed to ensure that the level of medium would not change during the experiments. Characterisation of the chambers was also performed prior to cell adhesion with solution A in order to verify the functioning of the chambers before EC measurements. These tests were also used to assess the variability of the impedance measurements from electrode to electrode and chamber to chamber.

## **3.2. Chambers characterisation**

### **3.2.1. Leakage test and sterility**

A preliminary study was carried out during which the performance of the existing chamber design used previously within the lab was assessed. It was found to have a number of limitations including regular leakages and high risk of infection. Through a number of modifications to the design and manufacture, a second generation of chambers were developed. The methods in chapter two describe the optimised manufacturing procedure used to produce these chambers and the results presented in this chapter refer to these five chambers only (CH10-14).

No leakages were seen during the testing period used prior to the EC impedance measurements. During the subsequent EC impedance measurements no leakages were observed in any of the chambers.

No infections were observed during the whole process (Day1-Day6).

### 3.2.2. Impedance measurements in solution A

In total, 60 impedance measurements with solution A were performed, involving 3 repeat tests (A – B – C) per electrode (E1 – E4) for each, for each chamber (CH10-CH14). This section shows the variability of the measurements within the same electrode (repeatability), between the electrodes of the within the same chamber (intra variability) and between the chambers, (inter variability).

#### 3.2.2.1. Repeatability of impedance measurements

In order to test the repeatability, tests were carried out on each chamber to assess how precise the readings were with 3 consecutive tests on one of the electrodes. The results of this work are shown in table 3.1. The repeatability seems to be high on all the chambers as the variability is less than one percent.

Repeatability tests (a, b ,c) with solution A at 2 KHz.														
Solution A characterisation			Solution A characterisation			Solution A characterisation			Solution A characterisation			Solution A characterisation		
CH/Electrode	Test	Z  mod	CH/Electrode	Test	Z  mod	CH/Electrode	Test	Z  mod	CH/Electrode	Test	Z  mod	CH/Electrode	Test	Z  mod
chamber14e4a	A	287.05	chamber13e3a	A	233.91	chamber12e2a	A	207.14	chamber11e3a	A	205.54	chamber10e1a	A	410.45
chamber14e4b	B	287.19	chamber13e3b	B	234.32	chamber12e2b	B	207.29	chamber11e3b	B	205.48	chamber10e1b	B	409
chamber14e4c	C	287.31	chamber13e3c	C	234.43	chamber12e2c	C	207.49	chamber11e3c	C	205.4	chamber10e1c	C	409.07
AVERAGE =		287.2	AVERAGE =		234.2	AVERAGE =		207.3	AVERAGE =		205.5	AVERAGE =		409.5
STDEV.S =		0.13	STDEV.S =		0.27	STDEV.S =		0.18	STDEV.S =		0.07	STDEV.S =		0.82

**Table 3.1: Repeatability of the impedance experiments on solution A within the same electrode with three consecutive tests marked a, b, c. This is sample of each chamber for one electrode.**

#### 3.2.2.2. Variability of impedance measurements

In order to assess the variability of the measurements depending on the electrode and the chamber, we plotted the impedance values of each electrode for each chamber in the table 2 below. The values reported were obtained at a frequency of 1995 Hz.

Solution A characterisation at f = 1995Hz,  Z  values					
Chamber Number	CH10	CH11	CH12	CH13	CH14
Electrode 1	409	251	237	312	298
Electrode 2	248	218	207	244	255
Electrode 3	305	205	193	234	237
Electrode 4	304	220	220	240	287
Average of  Z	316.5	223.5	214.25	257.5	269.25
Std deviation of  Z	67.2	19.5	18.8	36.6	28.2
Relative error level	21%	9%	9%	14%	10%

**Table 3.2: variability of the measurements with solution A, within the same chamber. The relative error level was worked out by dividing the average of |Z| by the standard deviation.**



In table 3.2, chamber 10 and chamber 13 have the highest standard deviation. They are therefore the chambers which have the greatest variability from electrode to electrode. In contrast, chamber 11 and 12 have the lowest standard deviation score in variability. We can see that the electrode 1 and 4 of the chamber 14 are the two electrodes which have the closest values of  $|Z|$ . Figure 3.1 provides a brief comparison of the chambers in terms of electrode variability by comparing the averages of the 4 electrodes of each chamber. It is directly reflecting the data presented in table 3.2.

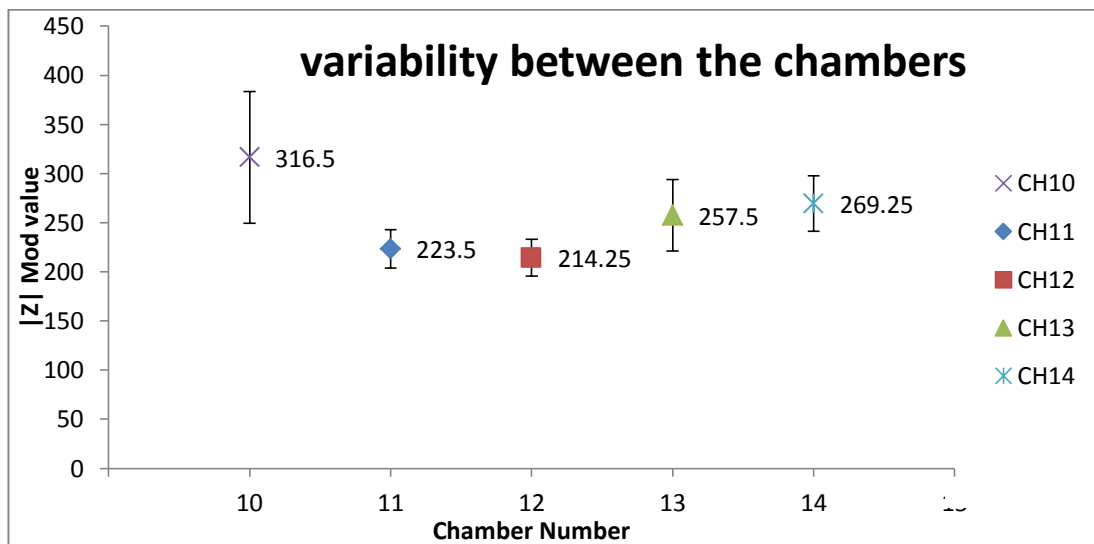


**Figure 3.1 Comparison of the intra variability of the 5 chambers. This is based on the average values of  $|Z|$  and their own standard deviations.**

We see easily that chamber 11 and 12 have the best characteristics in terms of precision because they have the smallest standard deviation and therefore the lowest relative error level in table 3.2.

A summary of the impedance signatures ( $|Z|$  vs Frequency) of the 4 electrodes of each chamber provided in figure 3.2. This highlights the linearity of the dataset in general and that the  $|Z|$  values of the electrodes tend to maintain their relationship to each other independent of the frequency in most cases.

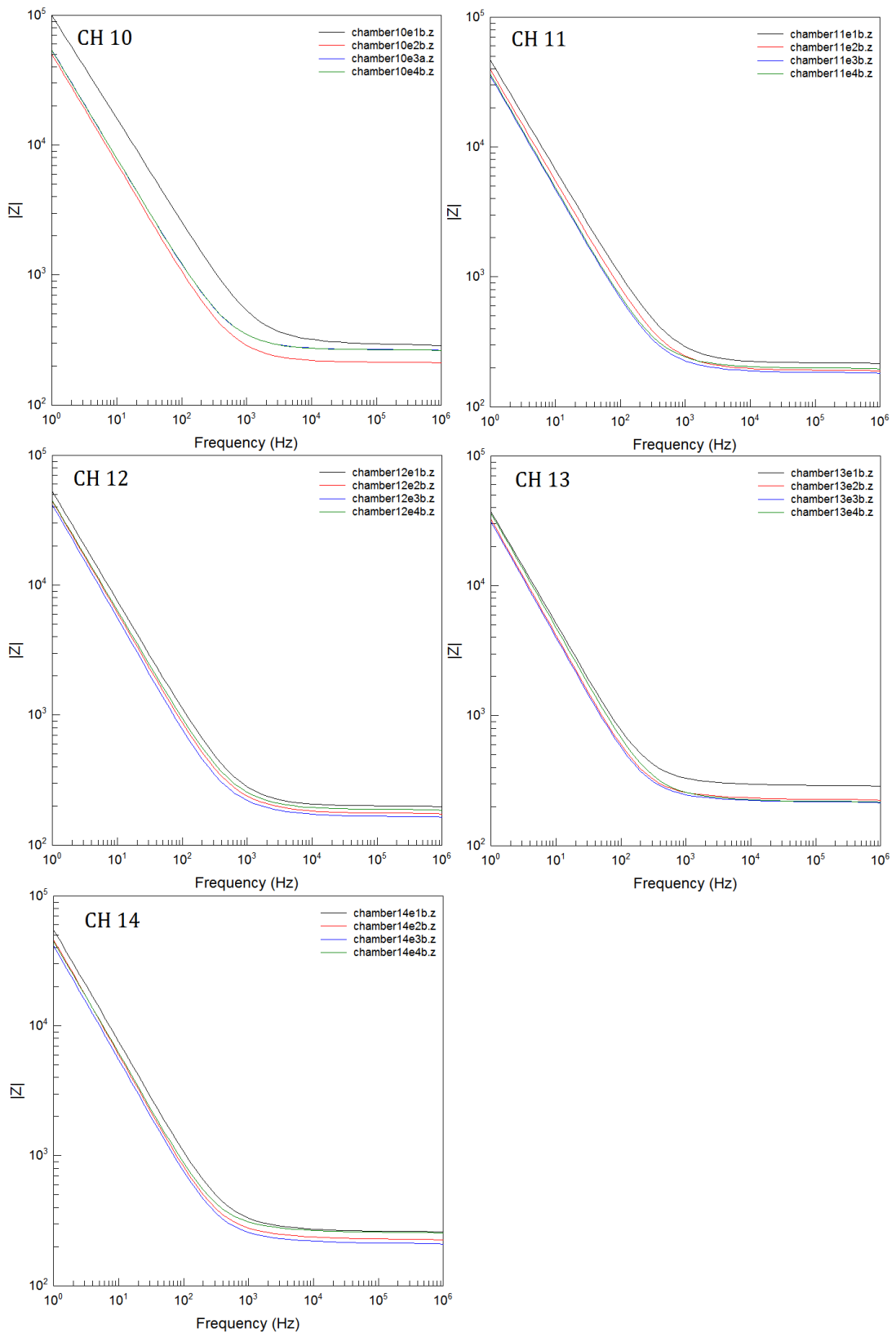


**Figure 3.2. Summary of the  $|Z|$  impedance values of the chambers measured in a wide range of frequencies (0Hz to  $10^6$ Hz). Each panel shows the  $|Z|$  values recorded for each electrode (E1 -E4) for the 5 bio sensor chambers (CH10 -CH14). All the 61 points of one line consist in one impedance signature or impedance profile**

In fig 3.2, the more the curves tend to merge in one thick line the lower will be the standard deviation score. The closer the values between the electrodes are, the less the data will be altered by the impedance values which are characteristic of the electrodes alone.

### 3.3. Impedance monitoring of cell cultures

A total of 80 bio-impedance measurements ( $|Z|$  vs frequency) were performed comprised of one measurement for each electrode pair (E1 – E4) per chamber (CH10-CH14), once a day on Day 1, Day 2, Day 3 and Day 6.

Chamber 10, 11, 12, and 13 were seeded as described in the previous chapter with endothelial cells at day 0. In the control chamber (chamber 14) no cells are present. The impedance measurements were taken at the following incubations times:

- Day 1 : 20 hrs after day 0
- Day 2 : 24,5 hrs after day 1
- Day 3 : 22 hrs after day 2
- Day 6 : 72 hrs after day3

Total: 138.5 hrs. Of incubation.

The medium was changed once, only after the impedance experiments on day 3 and it has to be mentioned that during day 2, an error in the setup led to the destruction of electrode 1 and 2 of chamber 11.

In order to examine the Z values of the cells in chambers, we first plotted the  $|Z|$  values versus the frequency  $f$  for the cell free control chamber 14. We displayed only a part of the graph here as a full scale would reduce visibility of small changes occurring. The graphs in figure 3.3 show each electrode of the control chamber and their decrease of impedance values, mostly from day 1 to day 2.

This can be seen across all the frequencies tested (an example is given in appendix A). It is clear that the reduction in impedance is the greatest from day

1 to 2. After this, the variation in impedance reduction evens out. Electrode 1 and 4 seem to have higher values than electrodes 2 and 3.

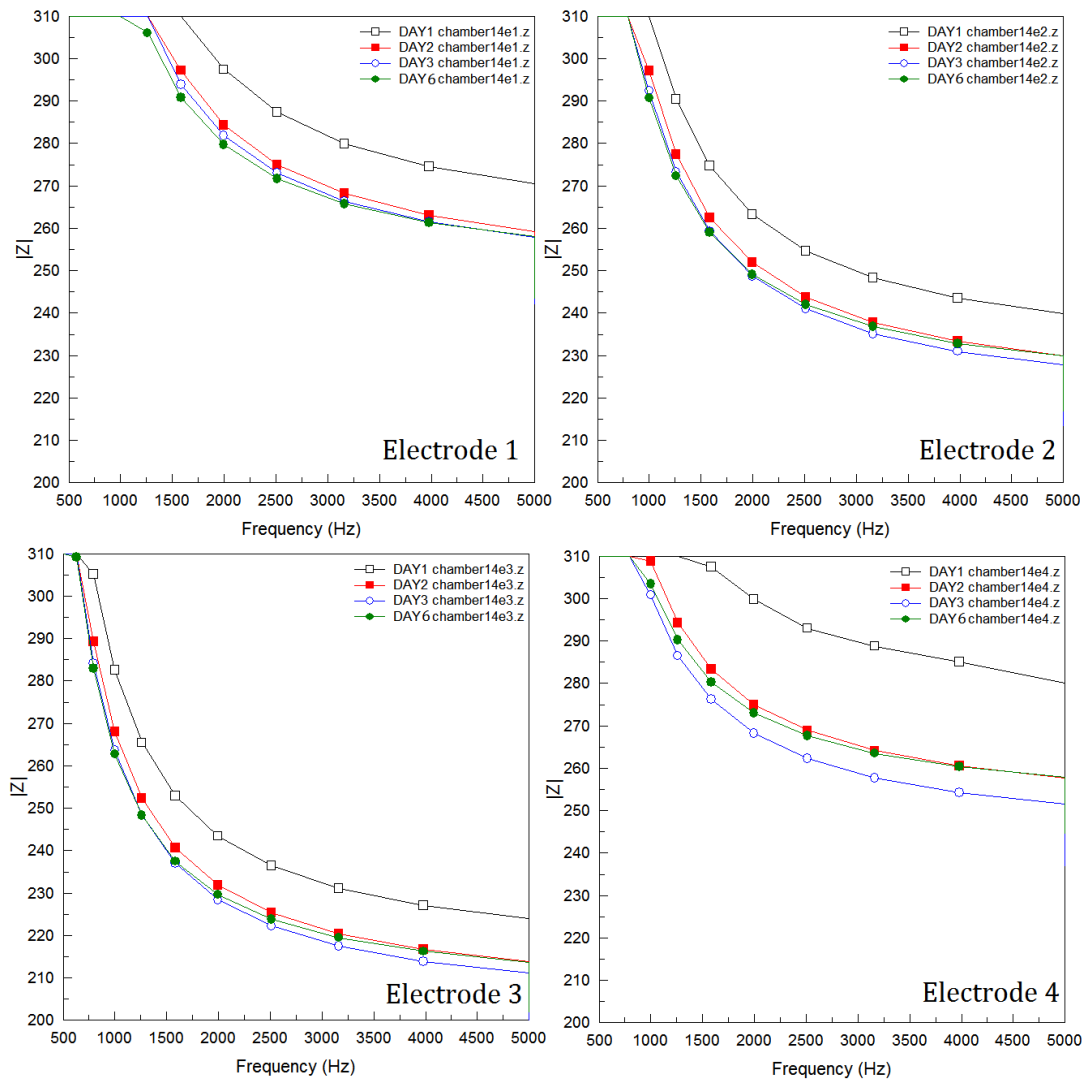


Figure 3.3 shows a summary of the  $|Z|$  impedance values of the chamber 14, measured in a focused range of frequencies (500Hz to 5000Hz). Each panel shows the  $|Z|$  values of chamber 14, recorded for each electrode (E1 –E4) for each experiment day (day 1, 2, 3, 6) with medium.

The scale has been reduced to the area of interest (2 KHz, as used the following measurements) because a full scale graph reduces visibility of small decreases in the  $|Z|$  values of the electrodes.

The impedance signatures of the four biosensor chambers containing cells (Ch 10 – 13) have all been compared with the cell free chamber (CH14) on each panel of the figure 3.4, for the 6 days of experiment.

Each point represents the average value of the 4 electrodes of one chamber at one particular day (day 1 – 6). In the figure 3.4 the  $|Z|$  values of the control

chamber without cells (common to all the panels) became stable from day 2 to day 6.

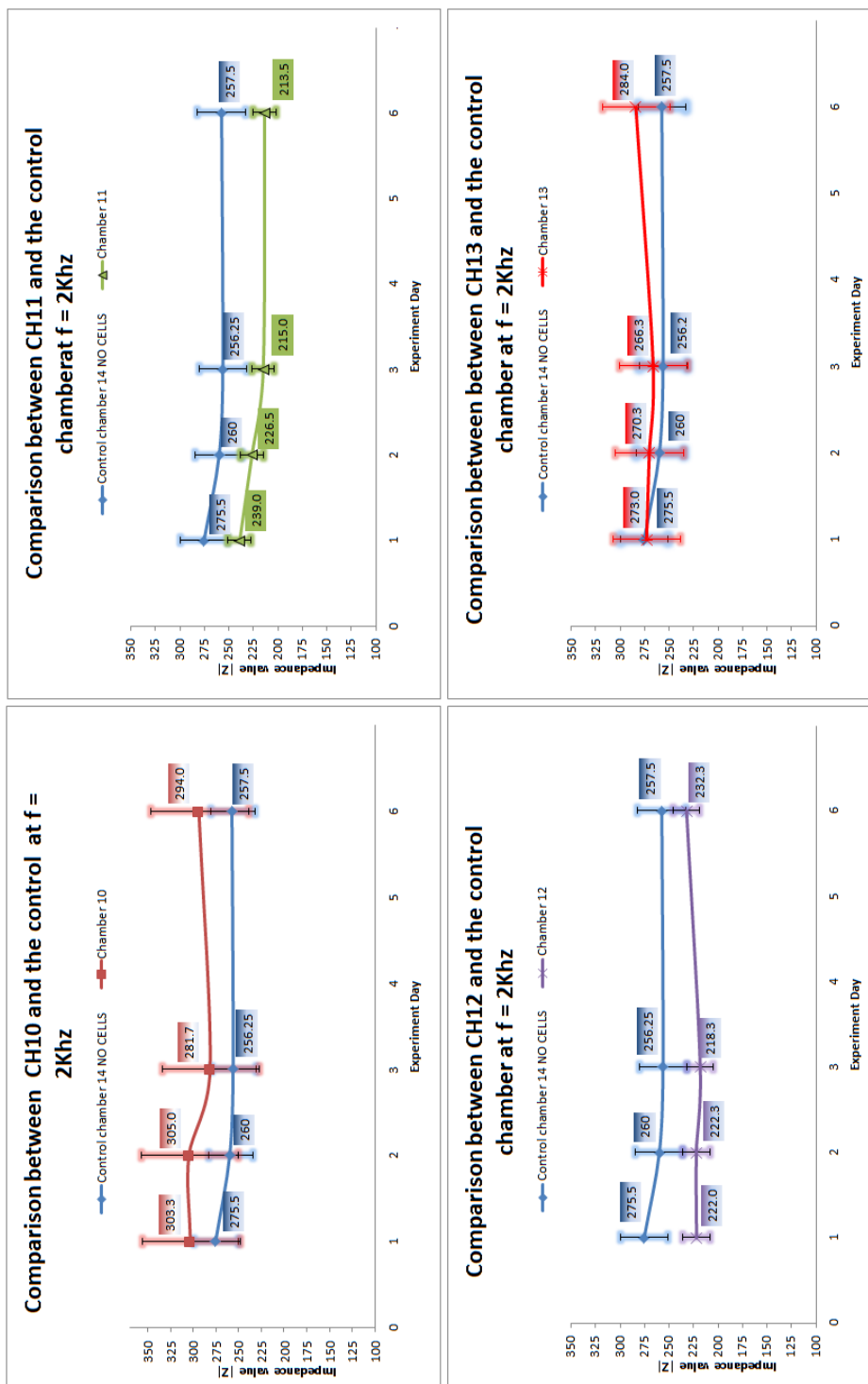


Figure 3.4: Shows average of |Z| values of the four electrodes from the four biosensor chambers containing cells (CH 10 – 13) compared with the cell free chamber (CH14, blue) over the 6 days of incubation. Each panel shows one chamber comparison. Each point represents the average value of the four electrodes of one chamber at one particular day (day 1 – 6).

Three other chambers with cells (CH 10, 12 and 13) exhibit a common feature; their  $|Z|$  values from day 3 to day 6 have increased.

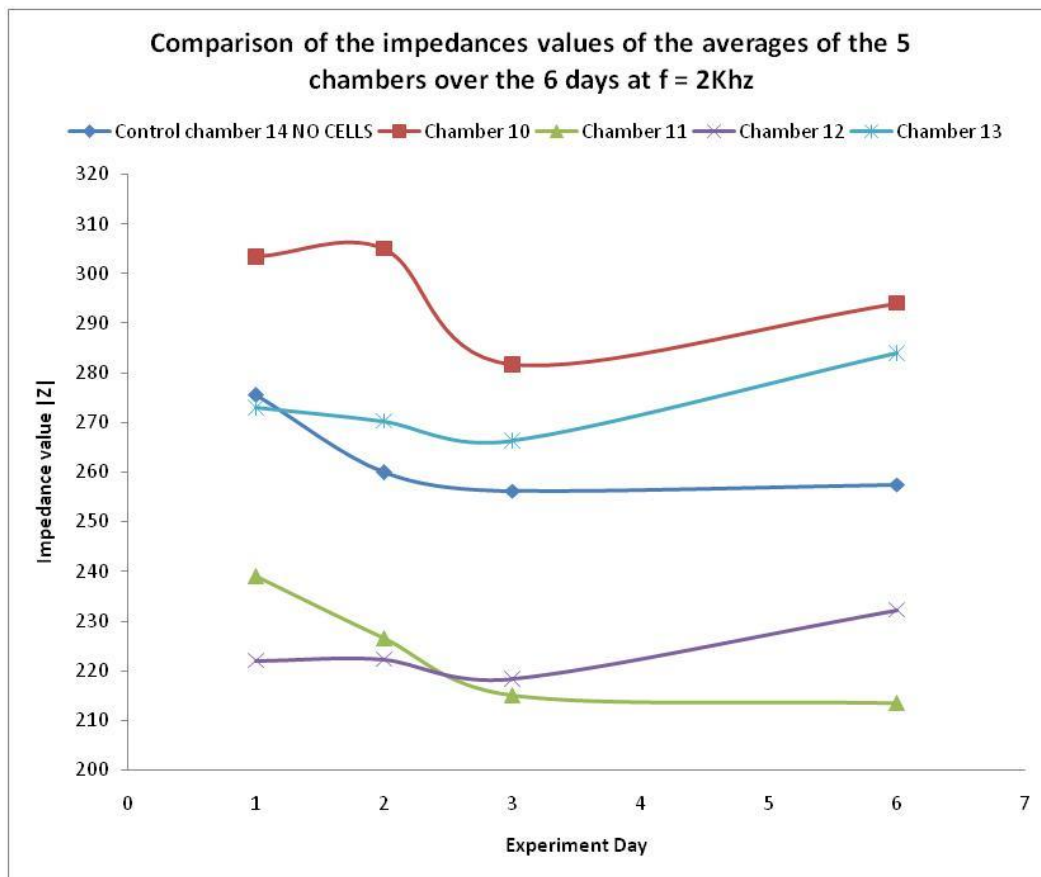


Figure 3.5 shows a summary of the  $|Z|$  value average of the 4 electrodes from the four biosensor chambers containing cells (CH 10 - 13) compared with the cell free chamber (CH14, blue) over the 6 days of incubation.

Figure 3.5 highlights the increase of their  $|Z|$  from day 3 to day 6 of the chamber 10, 12 and 13. The behaviour of chambers 11 and 14 seems to be highly similar.

Only one biosensor chamber with cells (CH11) did not follow the same increasing path of CH 10, 12, and 13 and rather follows approximately the same path as the control chamber. This may be explained by an error in the setup which caused a slightly higher current that may have generated morphological changes in the cells and damages to the electrode (see microscopy section, figure 3.10).

However in the figure 3.4 and 3.5, the chamber 11 and chamber 12 showed a lower level in their  $|Z|$  values compared to the control chamber, while chamber 10 and 13 have a higher value than the control chamber. A possible reason for this is that the solution A values of all the chambers (base values) follow the values of the endothelial cell experiment on day 1. In other words, these lower and higher levels are characteristic of the chambers and not the cell introduction. It is observable from figure 3.6 which shows a comparison between the measurements of the average values of  $|Z|$  on solution A and the endothelial cell growth on day 1.

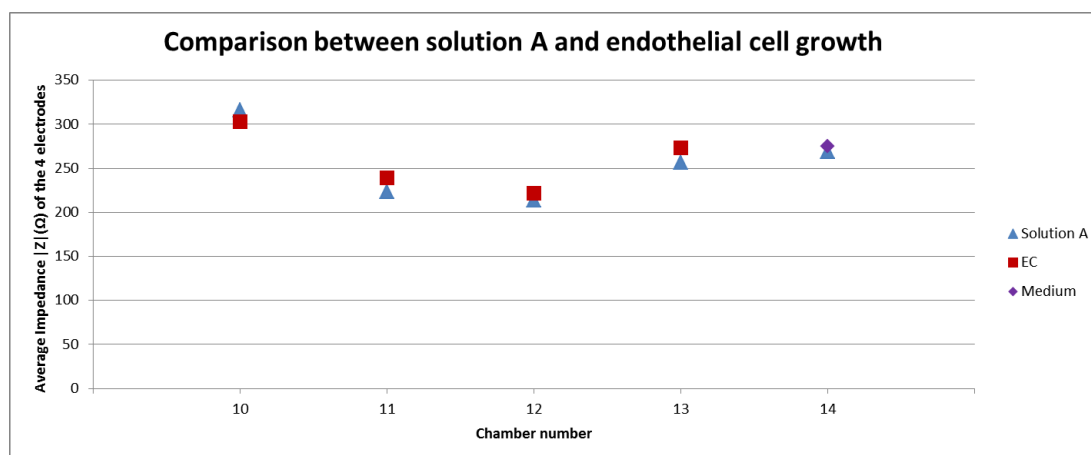


Figure 3.6: Shows averages of the  $|Z|$  values of the four biosensor chambers containing endothelial cells (CH 10 – 13), 24 hrs after seeding or medium (CH 14) 24 hrs. after seeding, compared with the solution A characterisation.

It is clear from fig. 3.6 that all the average values are not on the same level for both Solution A and EC. However, we can observe that 24 hours after seeding, the levels of EC follow very closely to the level of previously measured Solution A. This explains the observation of lower  $|Z|$  values on chamber 11 and 12, and higher values with chambers 10 and 13 in figure 3.4.

In order to establish a possible link between the average impedance of the chambers and the amount of cells present in the culture cube of the chambers, we plotted for each chamber the overall averages of the four electrodes measured throughout the full duration of the study against the estimate of the number of cells for each chamber (figure 3.7).

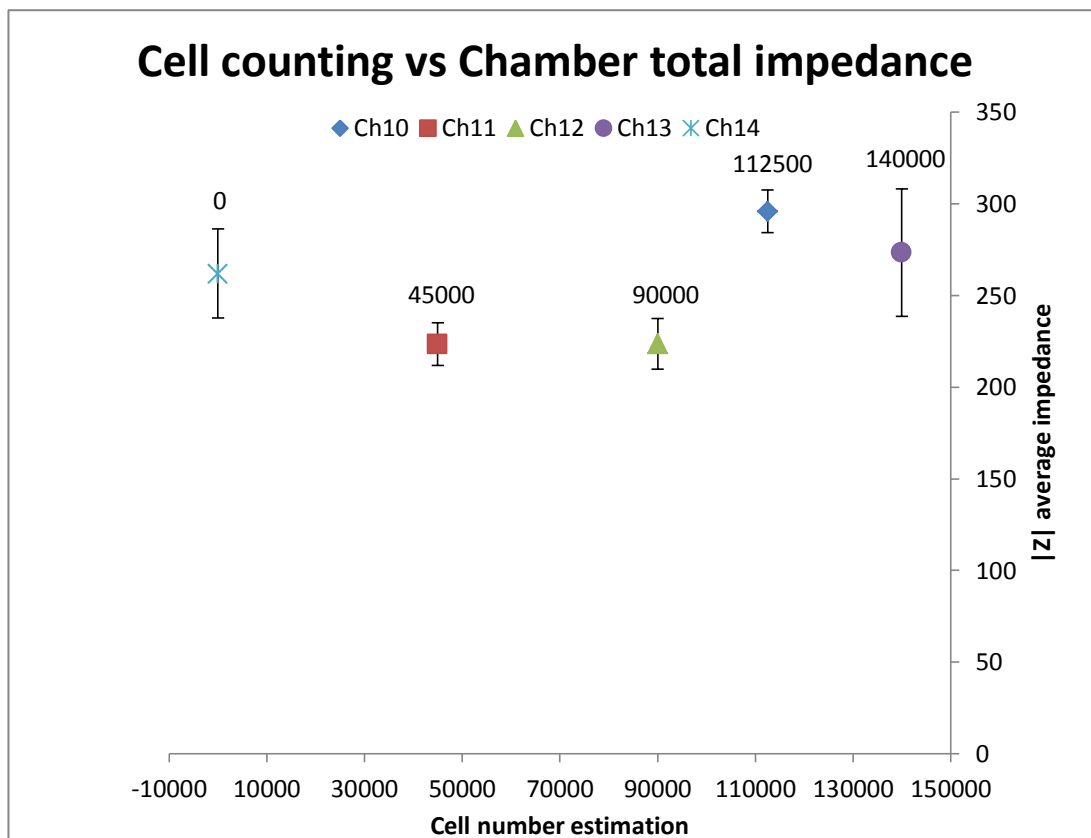


Figure 3.7: Shows general average of the  $|Z|$  values of the chambers against the estimation of the number of cells for each chamber. The labels above the markers show the estimated number of cells in the corresponding chamber.

In the above figure, there is no clear relationship observed between the  $|Z|$  values of the chambers and the cell estimation number. However it was recognised from the figure 3.6 that the base level of impedance on solution A of each chamber could be highly variable. This may present an explanation of the above observation. It was therefore decided to examine the impedance versus incubation time for three electrodes (figure 3.8) which had their  $|Z|$  values close to the control chamber, more specifically those that were within a tolerance of  $\pm 3\Omega$  of the control chamber.

These have been organised by suitable pairs:

- Pair 1 : chamber14e3(**237  $\Omega$** ) & chamber13e3 (**234  $\Omega$** ) (delta = -3)
- Pair 2 : chamber14e3 (**237  $\Omega$** ) & chamber12e1 (**237  $\Omega$** ) (delta = 0 )
- Pair 3 : chamber14e3 (**237  $\Omega$** ) & chamber13e4 (**240  $\Omega$** ) (delta = 3 )



In other words, these specific pairs have the best characteristics to be compared because their original impedance profiles are similar.

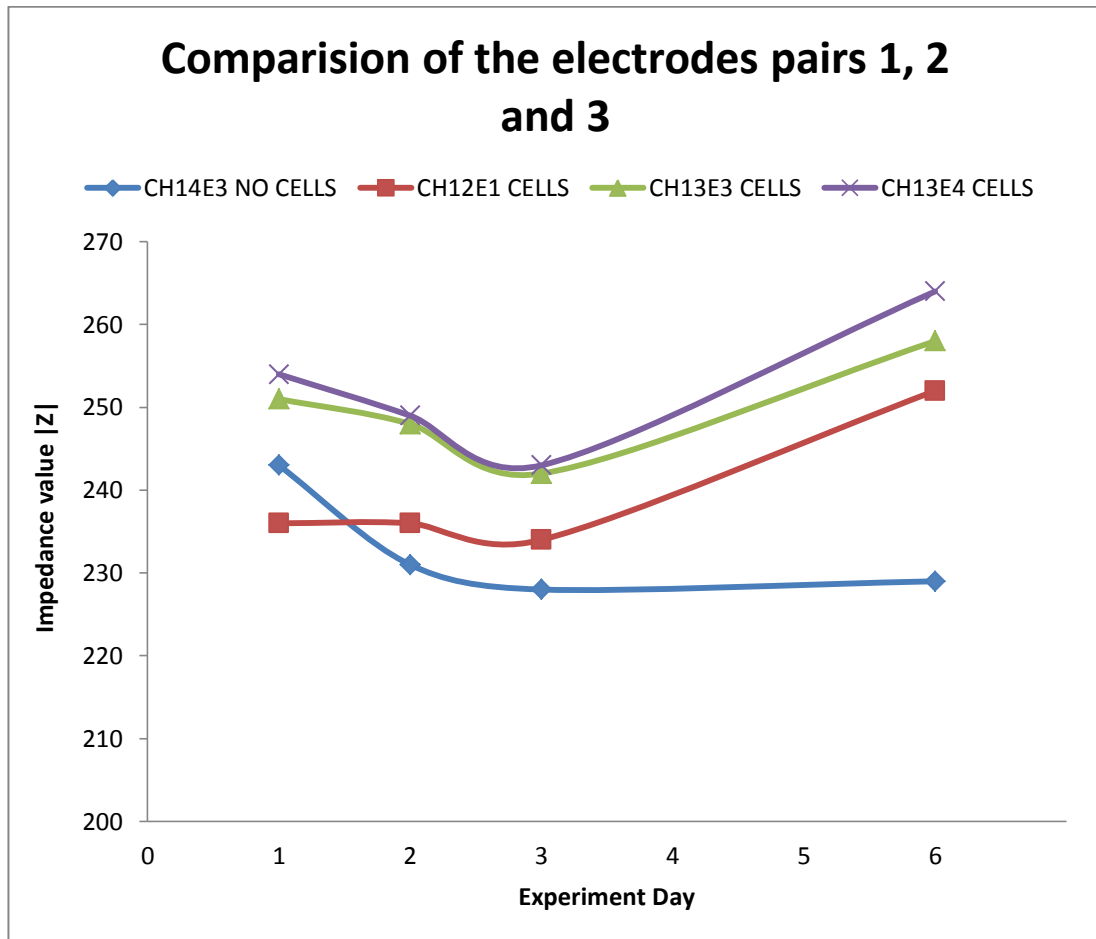


Figure 3.8: Shows a comparison of the measured  $|Z|$  values against the experiment day of the selected electrodes: Pair 1: chamber14e3 & chamber13e3, Pair 2: chamber14e3 & chamber12e1, Pair 3: chamber14e3 & chamber13e4. The scale has been adapted in order to distinctively visualise the increase in impedance.

The figure 3.8 shows clear differences between the chambers with cells and the control chamber without cells. While the control chamber remained stable from day 3 to day 6, the three other chambers increased their  $|Z|$  values (CH13E4, +8.6%; CH12E1, +7.7%; CH13E3, +6.06%). We therefore plotted the value of those three electrodes against the estimated number of cells on day 6, in order to confirm the relation between the impedance and the cell estimation number.

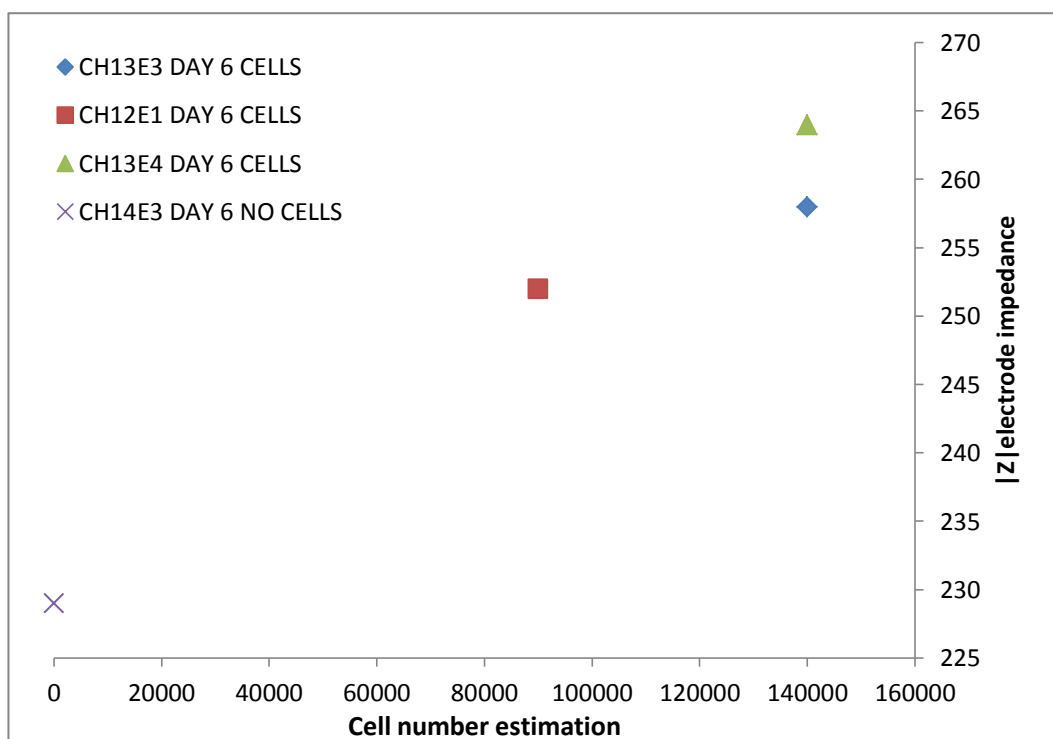


Figure 3.9: Shows the relation of the  $|Z|$  values and the cell number estimation, between the 3 cell culture chambers from figure 3.7 (CH13E3 CH12E1 and CH13E4) compared to the cell free chamber (CH14E3).

Figure 3.9 highlights existence of the relationship between the number of cells estimated and the impedance. This provides evidence (along with the figure 3.4) that our study is supported by the theory introduced in chapter 1.

### 3.3.1. Biosensor Microscopy

In this section, the most representative and distinctive images of each chamber on one electrode have been selected to show the endothelial cell proliferation over the 6 days of the experiment. As well as the data, no images are available from days 4 and 5 because of limited lab access over the weekend.

The images aim to support the data analysis previously shown and especially the proliferation over the electrodes of the endothelial cells.

In the pictures the gold electrodes are always in the middle (see the dotted line in figure 3.10 image E & A for better understanding) and the cells are seen through because of the thinness of the layer of gold.

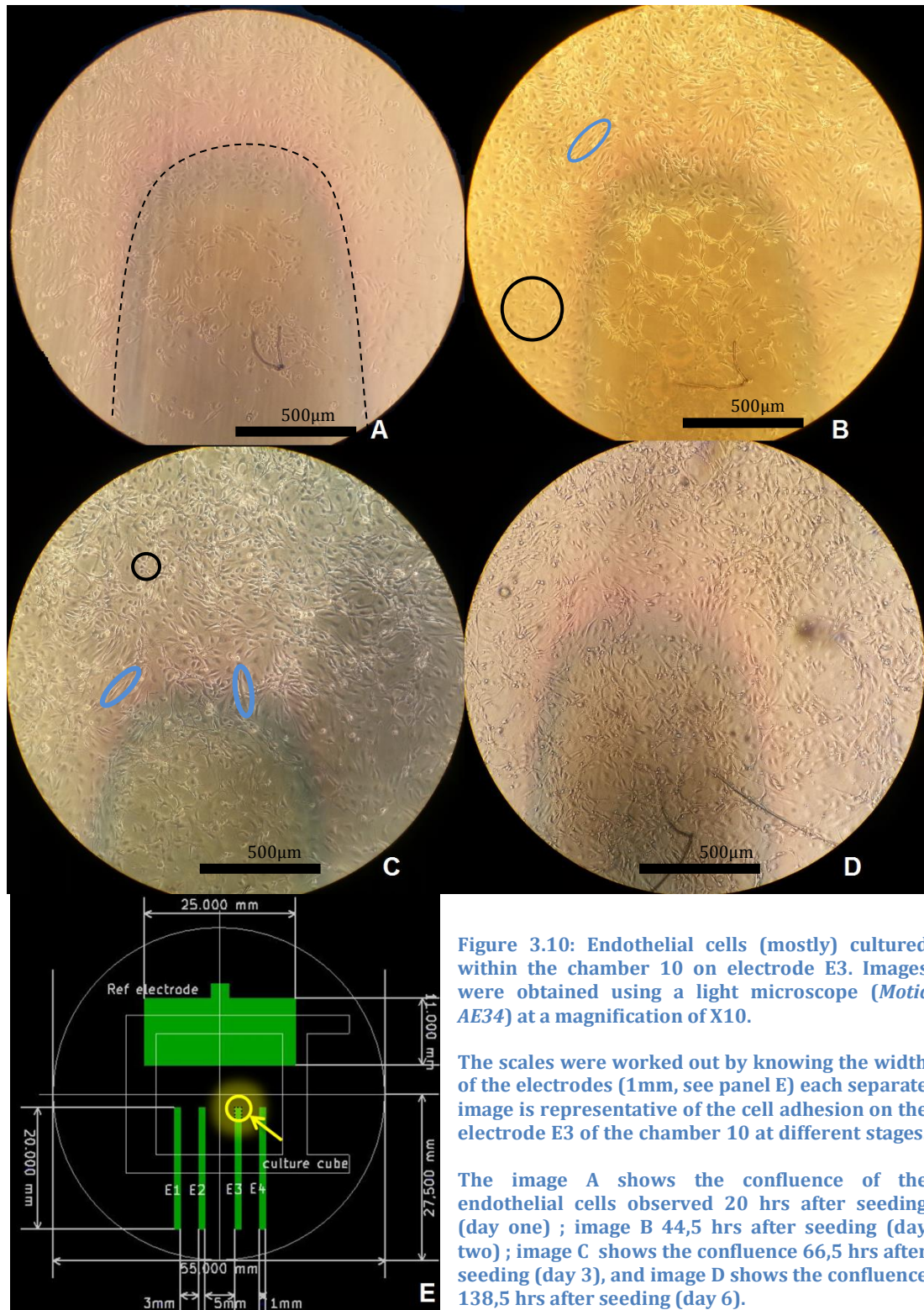


Figure 3.10: Endothelial cells (mostly) cultured within the chamber 10 on electrode E3. Images were obtained using a light microscope (*Motic AE34*) at a magnification of X10.

The scales were worked out by knowing the width of the electrodes (1mm, see panel E) each separate image is representative of the cell adhesion on the electrode E3 of the chamber 10 at different stages.

The image A shows the confluence of the endothelial cells observed 20 hrs after seeding (day one) ; image B 44,5 hrs after seeding (day two) ; image C shows the confluence 66,5 hrs after seeding (day 3), and image D shows the confluence 138,5 hrs after seeding (day 6).

In the image A the borders of the electrode are surrounded by a discontinued line, and this is visible as well in the image E which shows a plan of a chamber, (Which refers to the fig 2.4). In this plan the yellow highlighted circle indicates where the area of the other images (ABCD) was captured.

The black circles indicate what is thought to be endothelial cells and the blue oval closed curves are indicating cells which can be potentially fibroblast or smooth muscle cells. Image E designed with the open source software KiCad EDA Software Suite, 2014.

In the figure 3.10, electrode E3 of the chamber 10 exhibits a good example of a noticeable evolution in the cell confluence, especially between the images A, B, and C, where the cells are gradually covering the electrode. The plan on the panel B helps to indicate the exact location of the area where the other pictures are taken.

In the image C of the figure 3.10, various cell morphologies are noticeable such as cuboidal and spindle shapes. Those differences are due to the fact that various cell types can be present while collecting the endothelial cells from the freshly excised porcine pulmonary artery. This variation in cell types is therefore present in all the cultures of the biosensor chambers.

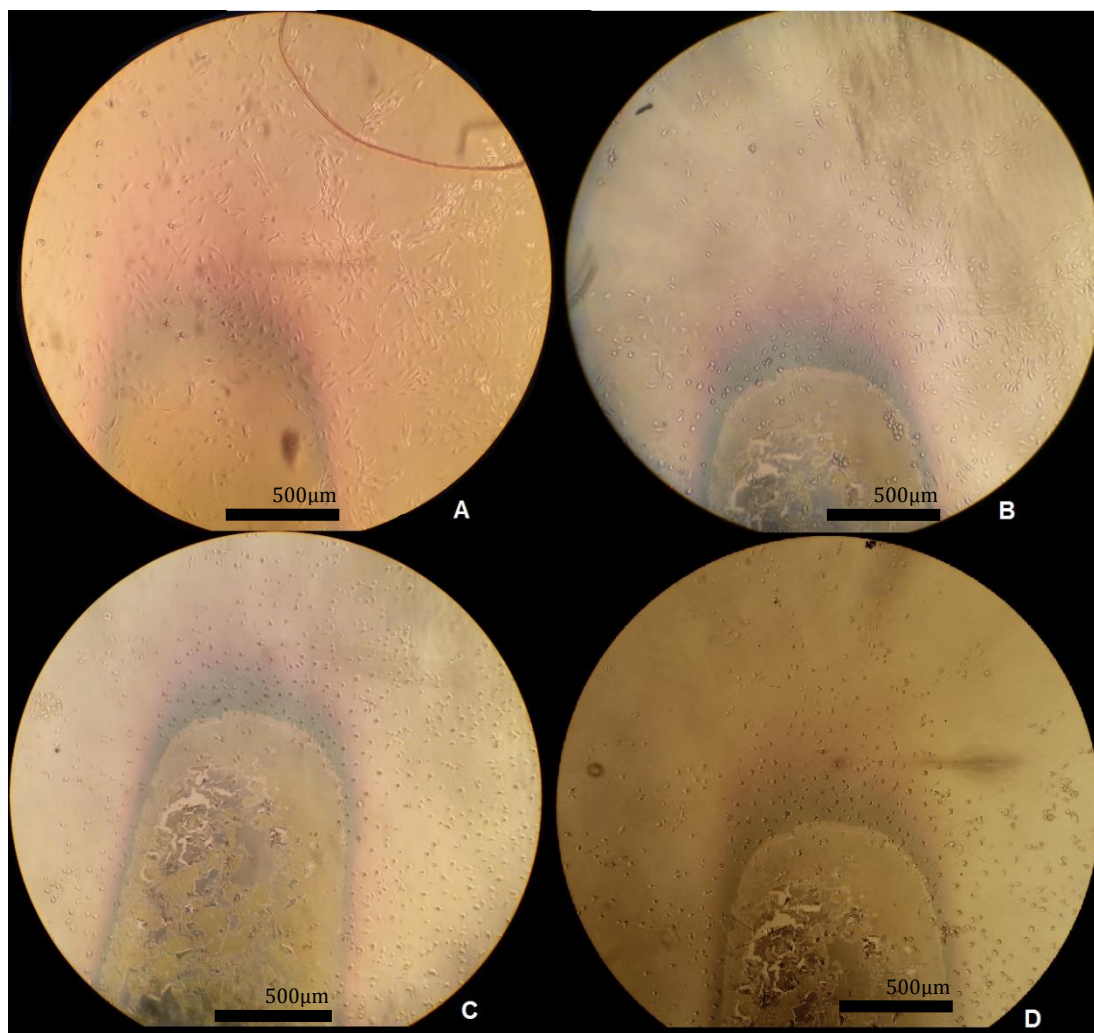


Figure 3.11: Endothelial cells cultured within the chamber 11 on electrode E1. Images were obtained using a light microscope (*Motic AE34*) at a magnification of X10. Each separate image is representative of the cell adhesion on the electrode E1 of the chamber 11 at different stages.

The image A shows the confluence of the endothelial cells observed 20 hrs after seeding (day one) ; image B 44,5 hrs after seeding (day two) ; image C shows the confluence 66,5 hrs after seeding (day 3,) and image D shows the confluence 138,5 hrs after seeding (day 6).

In the panel A the cells seem to be growing as in the other chambers 10, 12, and 13. B: after a high current passage, the electrode is damaged and the cells seem to undergo morphological changes. The same occurred during the other days.

In the figure 3.11 it is possible to see the damaged electrode of the chamber 11 which were provoked by an error in the settings of the impedance analyser.

This led to an increased current being delivered across two electrodes (E1 and E2 of chamber 11) during impedance measurements on day 2. This high DC current appears to have produced morphological changes in the entire cell culture, and may reasonably have been expected to have significantly damaged

the cells and the electrode. It is therefore not surprising that this chamber exhibited different results from the other chambers with healthy endothelial cells.

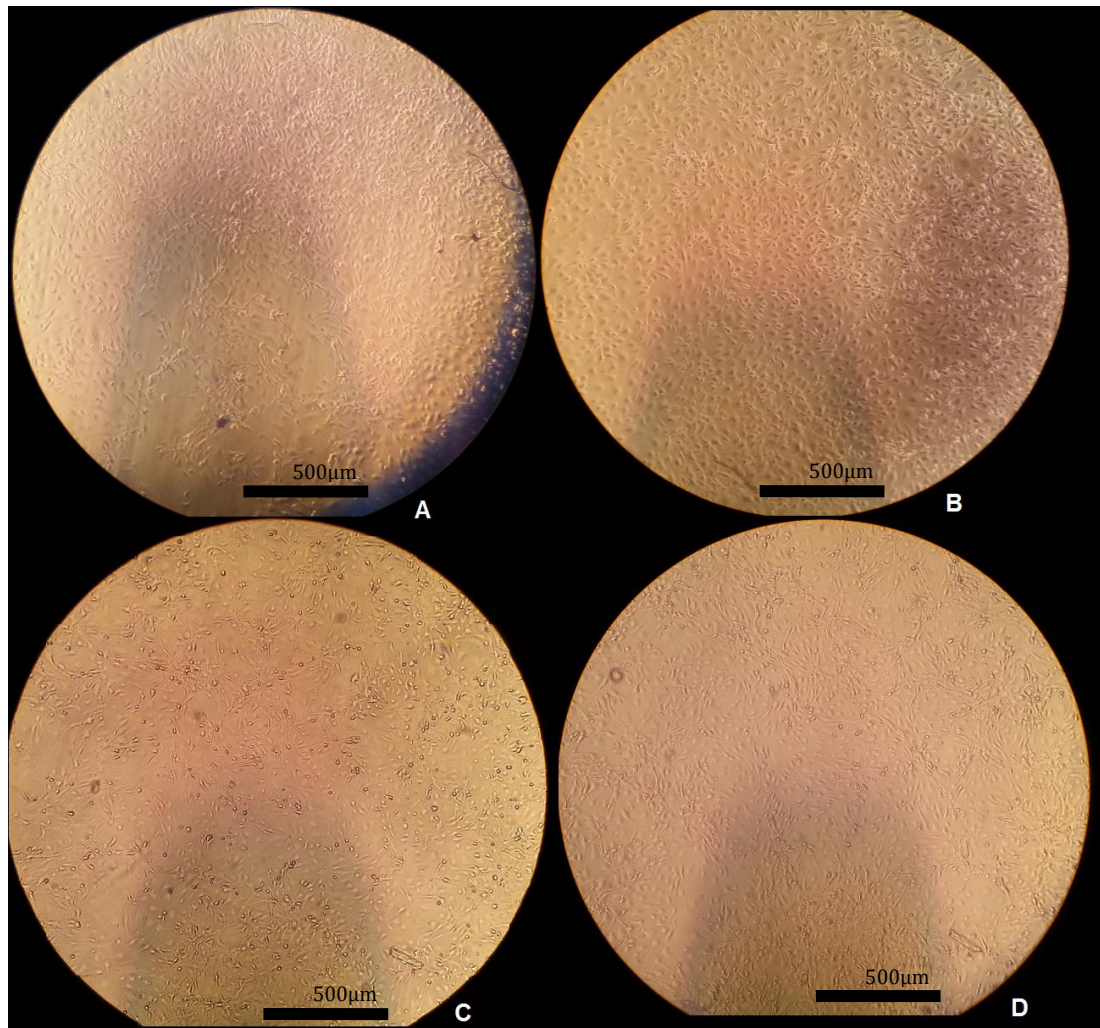


**Figure 3.12: Endothelial cells cultured within the chamber 12 on electrode E2. Images were obtained using a light microscope (*Motic AE34*) at a magnification of X10. Each separate image is representative of the cell adhesion on the electrode E2 of the chamber 12 at different stages.**

**The image A shows the confluence of the endothelial cells observed 20 hrs after seeding (day one) ; image B 44,5 hrs after seeding (day two) ; image C shows the confluence 66,5 hrs after seeding (day 3,) and image D shows the confluence 138,5 hrs after seeding (day 6).**

The figure 3.12 exhibits a certain evolution in the confluence between the day 1 (A) to the day 2 (B) on the electrode. However the confluence of the cells on the electrode seems to be generally high during the 6 days of experiments.

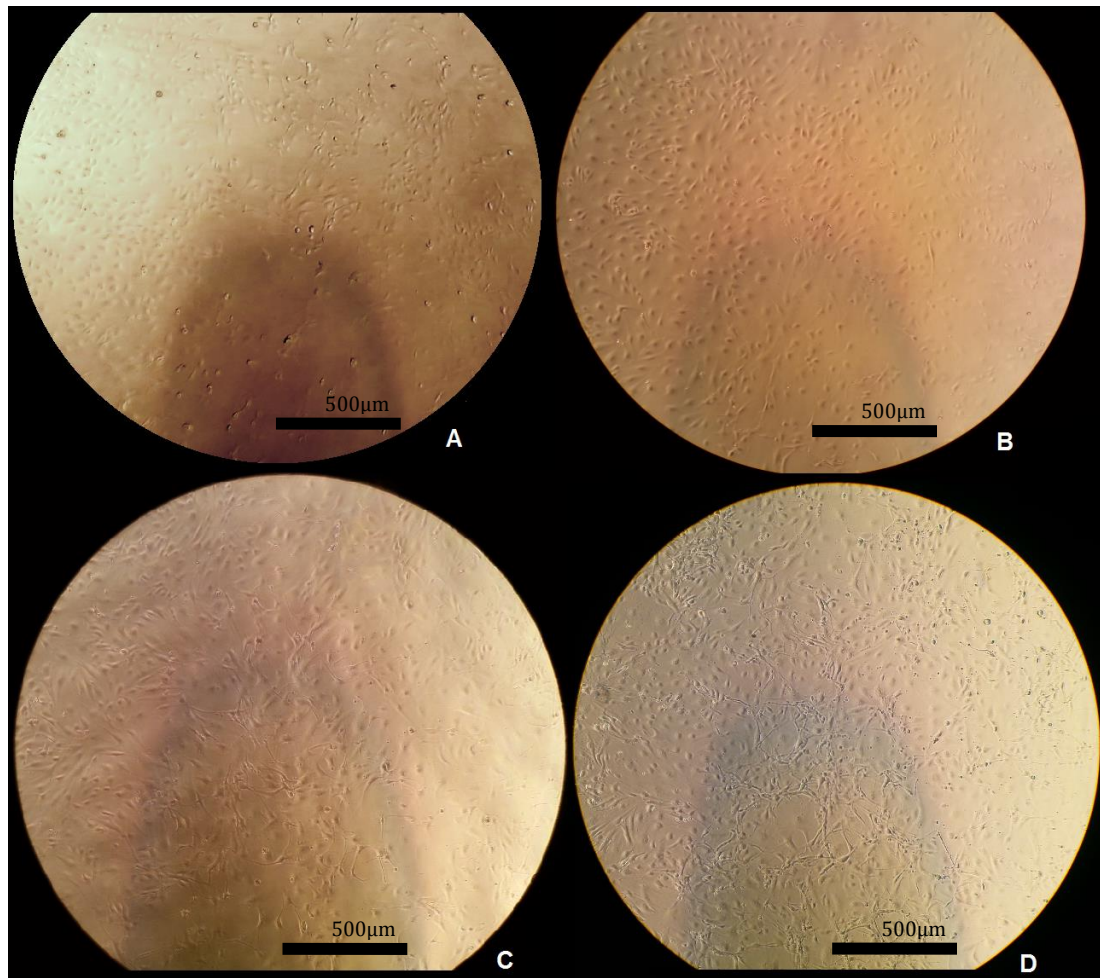


Figure 3.13: Endothelial cells cultured within the chamber 13 on electrode E3. Images were obtained using a light microscope (*Motic AE34*) at a magnification of X10. Each separate image is representative of the cell adhesion on the electrode E3 of the chamber 13 at different stages.

The image A shows the confluence of the endothelial cells observed 20 hrs after seeding (day one) ; image B 44,5 hrs after seeding (day two) ; image C shows the confluence 66,5 hrs after seeding (day 3,) and image D shows the confluence 138,5 hrs after seeding (day 6).

In the figure 3.13, the cell confluence observed on the electrode E3 of chamber 13 is gradually rising over the time. It is a nice example of the cell confluence development and this behaviour fits with the impedance signatures recorded on the figure 3.8 in the previous section.

### 3.4. Stent chamber experiment

The impedance measurements on the coronary stent involved one bare metal coronary stent (2.75 x 11mm Gazelle™ Biosensor International, Singapore) placed in one special chamber called the stent chamber.

In total, 9 impedance measurements with endothelial cells were performed on the stent chamber, involving one measurement per electrode (E1, E2, E1-2,) for each day of experiments (Day 1 – 3). See figure 2.7 in the chapter Methodology for the electrode arrangement.

Caution should be taken in the interpretation of the results from these following tests, since no control chambers were used, and no characterisation tests were performed prior to cell seeding.

The stent chamber started to leak on the day 2, and continued to until the end of the experiment. However, the medium was changed each day and kept at the same level in order to not alter the impedance values recorded.

The figure 3.14 shows the raw data of all the electrodes E1, E2 and E1-2 of the stent chamber from 0 to 1MHz. Only the impedance profile of E1-2 on day 3 differs clearly from the others on this graph, by exhibiting more linear behaviour across the wide range of frequencies. The other days of the electrode 1-2 are not present as they were completely out of range and therefore obscured the other impedance profiles.

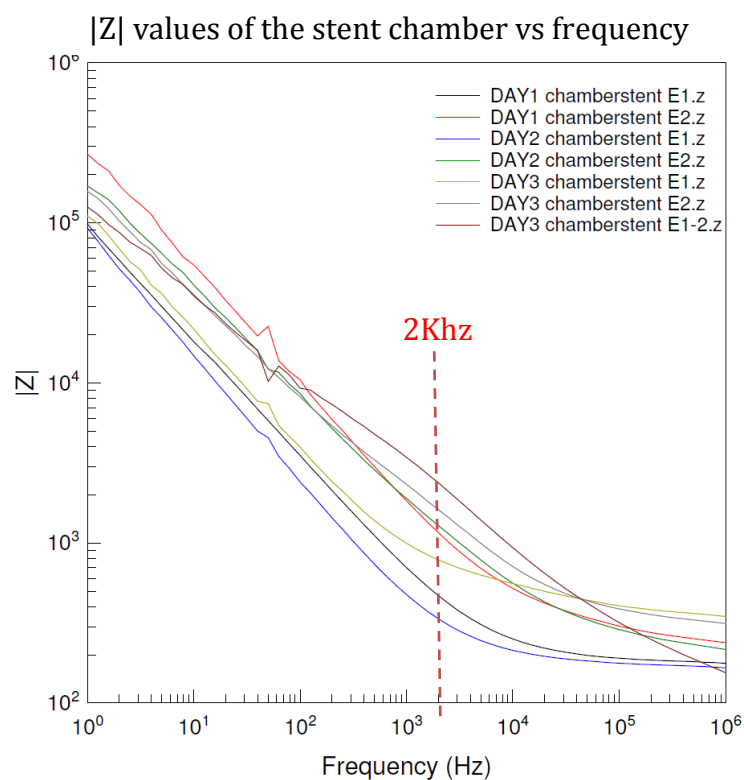


**Figure 3.14: |Z| impedance values of the electrodes of the stent chamber measured across a wide range of frequencies (1 MHz). Perturbations can be seen as little peaks around 50Hz, these are interferences due to the electrical network which provides a 50Hz alternative current for the operating devices connected around.**



However, it is difficult to clearly see the possible evolution in the impedance values  $|Z|$  over the days of each electrode. Therefore the  $|Z|$  values at fixed frequencies of 2 kHz were plotted against incubation time (figure 3.15).

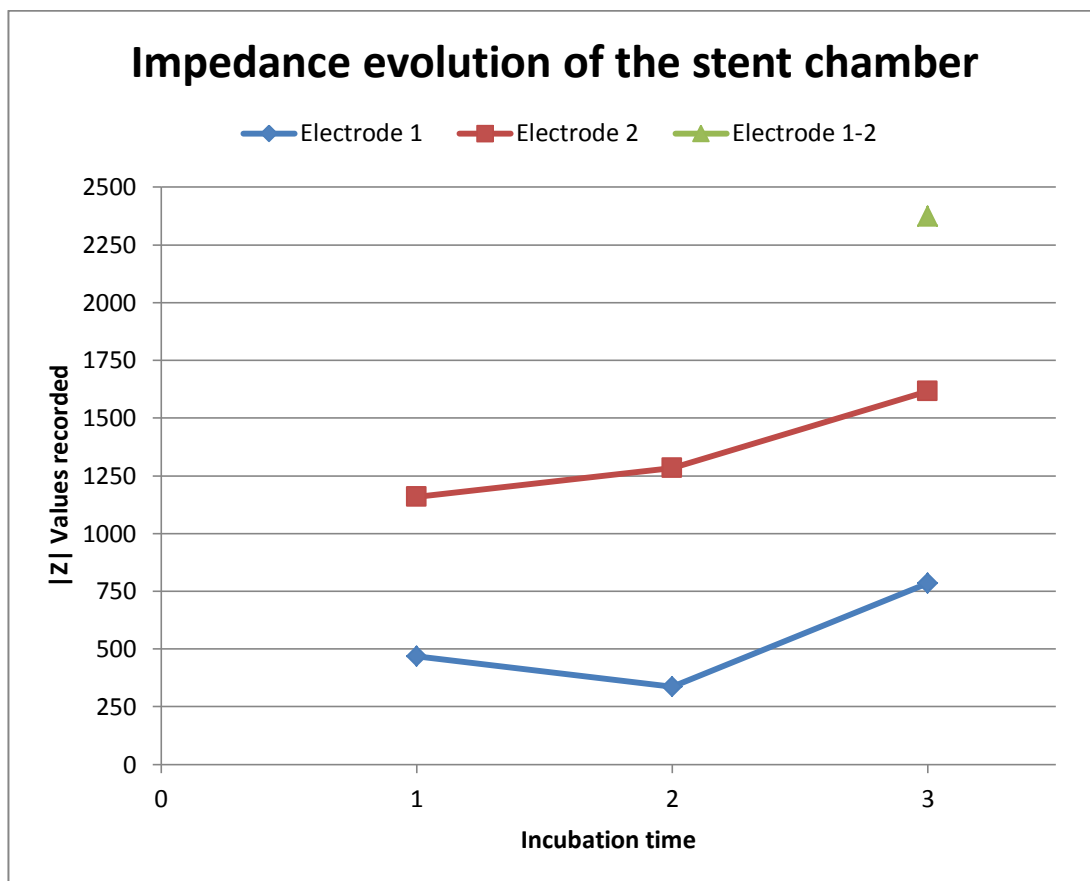


Figure 3.15  $|Z|$  impedance values of the electrodes of the stent chamber measured at 2 kHz over the 3 days of incubation. Only one value is available for electrode 1-2 at this frequency.

In the figure 3.15, it is now clear that there was an increase in the impedance values at 2 kHz over the 3 days of incubation. The electrode 1-2 is higher than the rest of the set.

### 3.4.1. Stent microscopy

In order to correlate the results with a possible coverage of the cells on the stent, close-up pictures were taken on the last day of experiment (figure 3.16) with light microscopy. Only a small percentage of what is thought to be cell coverage on the stent was observed although the cells were growing in the chamber with a high confluence. The fluorescent microscopy will confirm this

and provide a better idea of the real coverage of the stent by highlighting live cells.

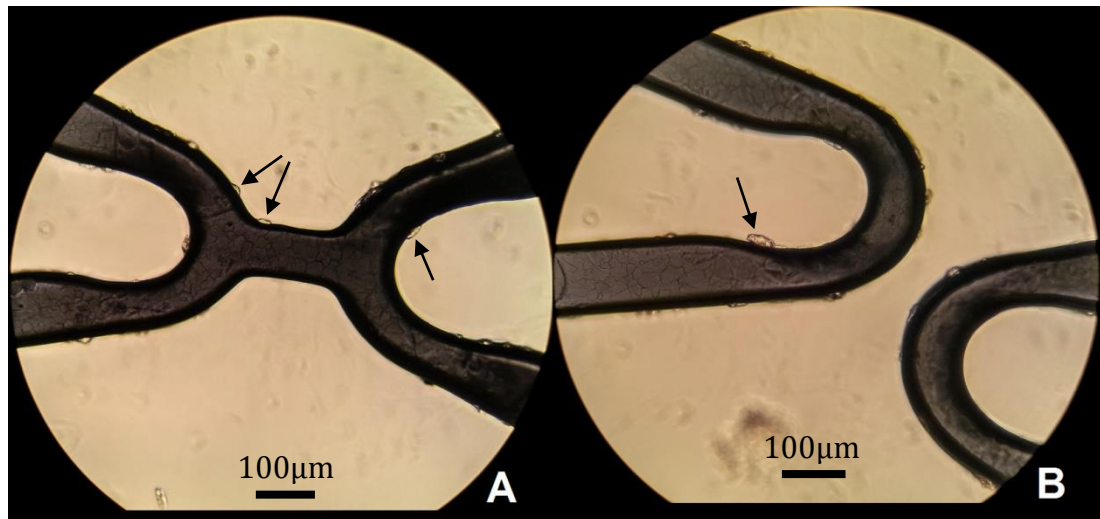


**Figure 3.16:** Light microscopy (MoticAE34 ) of the struts of the coronary stent on the stent chamber 72h (day 3) after seeding endothelial cells. The arrows the images A and B show what is thought to be living cells growing on the stent. Fluorescent microscopy can confirm this with a stained solution. The scales in this picture were worked out from the fluorescence microscopy by measuring the thickness of the stent's struts. Image captured thanks to a personal technique.

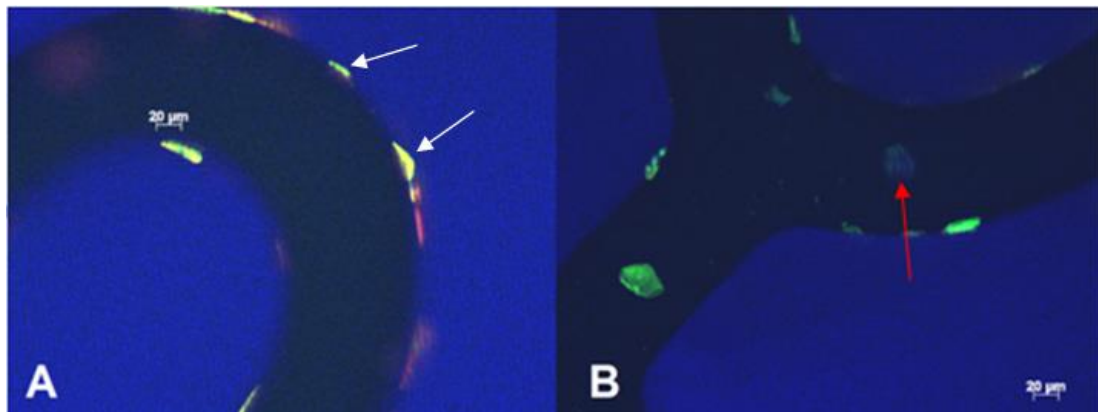


**Figure 3.17:** Fluorescence imaging of fixed samples (stained with acridine orange) on the struts of the coronary stent. This indicates that a small number of cells attached to the struts. The white arrows on the image shows a stained cell while the red arrow indicates what is likely to be an artefact due to non-specific staining. Scales and images from Zeiss™ Axioimager fluorescence microscope, Germany. The scale is 20µm.

Fluorescence microscopy was performed in order to distinguish cells from other possible compounds observable on the stent . In the figure 3.17, the white arrows on image A shows the presence of what may be a small number of stained cells (acridine orange) attached to the stent, while the red arrow shows a non-stained element. In the figure 3.16 those elements aimed by the red and with arrows would not have been distinguished.

The percentage of confluence on the Surface of the stent has not been calculated. We observed that the % of confluence of the endothelial cells is certainly less than 10%, however there is here little evidence for this percentage estimation and the cells have not been counted for this experiment.

## 4. Discussion

## 4.1. Chapter Overview

The overall aim of this thesis was to assess and monitor by impedance measurements endothelial growth on metal materials over time and the specific objectives previously addressed are discussed in the following sections. A brief resume of the key achievements are listed below and will be seen in details in the next sections.

The first objective was to develop 5 optimised culture chambers in order to record impedance measurements of EC growth. It was successfully achieved and we therefore then aimed to characterise them, in order to understand their behaviour in terms of impedance of each of them. We used for that a test solution called solution A. The results with this test solution demonstrated that the self-manufactured chambers exhibited a degree of variability that we had to consider in interpreting the results from further measurements. Endothelial cells were then cultured in order to seed the future chambers and record the bio-impedance for around one week duration. The impedance profiles of the cells were then compared to the cell count relative to the chambers in order to test the theory of the first chapter, which claims that the degree of coverage must follow the rise of impedance observed. Finally, the applicability of the methods used was tested on a coronary stent.

## 4.2. Objectives

### 4.2.1. Optimised biosensor chambers development

In this study, a series of biosensor chambers were developed and shown to be suitable for endothelial cell cultures and impedance measurements. The final five biosensor chambers produced and used in this study had no evidence of infection after 6 days in standard cell culture conditions. This was in contrast to the earlier generation chambers developed in preliminary work carried out during the developmental stage of this study, where first generation biosensor chambers were seen to be infected after only two days. Importantly, the low final rate of infection is an advance on the previous results gathered within the laboratory using similar devices (Shedden *et al*, 2008). The improvements made

to the chamber designs in the present study, notably the blockage of the holes of the chambers and the UV sterilisation prior to seeding the cells, are thought to be associated with this lower rate of infection. Similarly, no leakages have been reported during the characterisation and the endothelial cell growth experiment, in contrast with the previous generations of biosensor chambers. This is likely to be linked with the attachment method, which was a biocompatible double tape. In order to ensure that the edges of the double face tape were not altering the cell growth, they were analysed under the microscope and no alterations were found.

#### **4.2.2. Characterisation of the biosensor chambers.**

During the characterisation of the chambers, the repeatability tests showed a very small percentage ( $\sim 0.1\%$ ) of variation of the impedance  $|Z|$  values for consecutive tests on the same electrode. However these small changes might be caused by the repeatability tolerance of the measurement system. It was seen further in the results that the impedance changes caused by the endothelial cell growth were of a much larger scale (see fig 3.7 as an example). This supports the fact that the biosensor is fully capable of measuring endothelial impedance changes occurring within the same electrode.

The average variation between the chambers exhibits differences in their base impedance values and in standard deviation. This is clearly seen in figure 3.1. In theory they should have the same impedance and the same standard deviation errors because the manufacturing process and the measurements methodology were the same. However, during the manufacturing process, the addition of small changes that may have been caused by human error in manipulation is thought to have influenced the differences between chambers. For instance, the contact glue used in welding (see figure 2.4) has resistive properties which depend on the quantity of matter used. The addition of such details in

manufacturing are likely to have a strong effect on the data recorded, especially during accurate and precise measurements.

However, the levels of variability between electrodes within the same chambers were roughly between 10% and 20% of their  $|Z|$  values (see table 3.2). This variability is constant at all frequencies measured, therefore this encourages the possibility of comparison along the whole range of frequencies.

### **4.2.3. Impedance measurements of endothelial cell cultures.**

During the 6 days of experiments on cell growth, we measured the impedance values  $|Z|$  of the biosensor chambers containing the endothelial cells and we observed that in general, the raw data does not always follow a clear and evident theoretical path, however several interesting findings have been recorded.

The figures 3.4 and 3.5 highlight an impedance evolution in chambers with cells (CH10-13) as opposed to the control chamber (CH14), which was comparatively more stable, especially between days 2 to 6. The impedance rise observed in the cell chambers support the theory introduced in chapter one regarding cell growth and the following impedance behaviour. This observation of cell growth is supported by the samples in the microscopy analysis (figure 3.10).

The chamber 11 is thought to support the two previous assumptions, as this chamber exhibits clearly different cell organisation and morphological changes due to increased current induced. On the other hand, the electrode was damaged as well, and therefore it is difficult to know the impact ratio of each of those two factors on the CH11 results.

The drop in the impedance in the control chamber 14 between day 1 and day 3 (figure 3.5) may be linked to protein adhesion (Moulton *et al.*, 2004) present in the media. This seems to stabilise after day 3 in contrast to the chambers with cells.

The cell count (estimation visible in fig. 3.7) compared with the average of  $z$  impedance values taken from all chambers shows that there was no clear relationship between impedance and the final number of adherent cells. This is in contrast to what was expected, based on other similar studies that have demonstrated that impedance increases with cell growth (Wegener *et al.*, 1996, Peting *et al.*, 1987). In order to investigate the reasons for this discrepancy, it was decided to compare impedance measurements made after one day of endothelial cell growth, with the solution A impedance profiles for the chambers. This analysis (figure 3.6) revealed that there was a large range of varying starting base values of impedance in solution A between the chambers. This large range of starting base values was observed to be the same with initial impedance measurements following endothelial cell seeding. This may in part explain the lack of correlation observed between the cell counting and chamber total impedance comparison. To reduce the impact of such variation, a small number of electrodes pairs with very low variability (similar  $|Z|$  values) and very close values from the electrode of the control chamber were selected for further analysis (see figure 3.8). In this small sample, the increase of impedance observed in the cell chambers clearly supports the original hypothesis (see section 1.9) that the impedance measurements would correlate with the degree of confluence of the cells proliferating. This is shown in figure 3.9, where we can see this correlation in cell growth over the six days of experiments. This supports the potential use of impedance as a method of monitoring the amount of endothelial cells on a metal surface.

Although it was intended that only endothelial cells be present within the cell cultures used in this study, it appears clear that there were also other cell types present. This can be seen in figure 3.10 (panel C) where a mixture of cuboidal



and spindle-like cells can be distinguished. The cuboidal cells are the more likely to be endothelial cells and the spindle ones are likely to be smooth muscle, fibroblast or other possible vascular cells. The presence of such cells is likely due to a small number of fibroblasts and smooth muscle cells being scraped off during the isolation method. Given the relatively high passage number used, the presence of significant numbers of highly proliferative cell types (smooth muscle and fibroblast) is perhaps to have been expected.

#### **4.2.4. Stent chamber experiment.**

This pilot experiment showed a certain impedance evolution over the three days of experiment (figure 3.15). This increase is not likely to be due to cell adhesion as the microscopy (figure 3.16 & 3.17) suggest that the cell coverage was very low.

One potential reason for this low level of endothelial cell coverage is thought to be caused by a lack of time for the cells to adhere to the stent, and also because the chamber experienced leakage problems during the 3 days of experiment.

We observed that the impedance values of  $|Z|$  were slightly higher in the stent chamber (300-2300 $\Omega$ ) (figure 3.15) as compared to the biosensor chambers (210-310 $\Omega$ ) and this is likely to be caused by the stent resistance and the differences in the apparatus, such as the reference electrode nature (immersed stainless steel).

In conclusion, we have seen that the stent chamber manufactured in this study was capable to measure impedance values, although there is no evidence in this study supporting the quality and repeatability of those measurements due to the experiment being an n of 1.

### 4.3. Limitations

In terms of chamber development, the hand manufacturing was a limitation because human error may cause random variations in the measurements. The lengths of the electrodes created via the mask were not exactly the same and not completely symmetric, as the mask was not properly optimised (hand manufacturing). This may have an impact on the different base levels of impedance measurements as the amount of gold defines the impedance of the electrode.

Considering the variability of the impedance values between the electrodes and the points previously discussed, it is likely that the sum of those errors leads to an overall error factor which has not been calculated.

The protein binding of the gold surfaces caused by the media or cell cultures discourages repeated use of the chambers, even if other studies did not consider this and used similar devices up to 20 times (Wegener *et al.*, 1996).

In terms of endothelial cell monitoring, the manipulations for the impedance spectroscopy were not performed in a sterile environment and this may increase the risks of infections. During the cell counting only two samples of 25µL each were counted per chamber. As we are assessing a technique which aims to monitor cell proliferation, a higher number of samples would give a better cell estimation. Another limitation is that the amount of cells counted is relative to the whole chamber cell culture. In the figure 3.9 we are comparing one impedance value of one electrode from a chamber to the estimated entire population of this chamber, therefore this comparison presupposes that the whole cell culture was completely homogenous. In order to perform a more precise comparison, only the cells which are involved in the current path should be counted.

Another limitation in the cell counting for the biosensor chambers is that the cells counted were not confirmed to be viable as no staining test was performed to assess their viability.

In terms of measurements, the number of chambers used in the experiments was small to ensure repeatable outcomes, and the first impedance measurement was carried out on day 1, 24h after seeding (day 0). This means that the cells already proliferated before the starting point.

In the figure 3.10, cells of different morphologies can be seen. Future work should involve the use of specific stains in order to distinguish cell types such as fibroblast and smooth muscle cells.

With the stent chamber, the absence of a control stent chamber did not allow direct comparisons such as the bio sensor experiments. The amount of data collected with this apparatus was very low, as only one chamber was tested and the duration of this experiment was short (3 days). An increase in duration to at least a week could be the base for further research. The cells should be counted and the coverage precisely estimated in order to make precise correlations between impedance and cell number.

#### **4.4. Future Research**

Future work on biosensor chambers development includes a higher precision of the device, using possible different electrode array patterns and a high repeatability in the manufacturing. An example of possible improved design for the electrode array is provided in appendix B. Considering that the electrodes are made from a thin layer of gold, it may be interesting to investigate the influence of the gold thickness as well as the effect of the special reliefs shown in appendix C.

A subsequent step following optimisation would involve replication of local conditions of the endothelial cells such as dynamic flow of medium while the cells are growing. It may be interesting to measure difference in terms of impedance in such an environment compared to a static one as used in this study.

Future research on endothelial cell monitoring with biosensor chambers may include a higher number of chambers tested in better measurement conditions, for example performing such tests directly in an incubator. The cell counting could be improved with a higher number of samples of cells taken and by using staining solution. Because of the time limitations previously discussed, it may be interesting to monitor the first hours of proliferation in order to observe a clearer impedance rise.

For the coronary stent, in addition of having to address all the key limitation points discussed before concerning the stent chamber, the use of impedance monitoring on coronary stents would involve different types of coatings in DES stents, as well as different shapes and sizes of the stent.

#### **4.5. Summary Conclusions**

The overall aim of this project was to assess and monitor by impedance measurements the endothelial growth on metal materials over time. The self-manufactured biosensor chambers were suitable for such recordings, but in a limited range of precision and repeatability. The impedances changes caused by the endothelial growth seen in the bio sensor chambers matched the theoretical concepts and were supported by microscopy analysis. The experiments based on endothelial cell growth demonstrated that impedance measurements were potentially suitable in quantifying the final number of adherent cells on gold planar electrodes using impedance monitoring. This was supported by a selection of electrodes which showed correlation between impedance measurements and the confluence of cells on their electrodes.

On the other hand, the results have to be considered with a range of variability. The pilot study on the coronary stent showed a certain possibility of measuring impedance and this encourages future studies to investigate the use of coronary stents in detecting endothelial cells growth.

## **5. Appendix**

## Appendix A: $|Z|$ impedance variability of the control chamber 14 with medium.

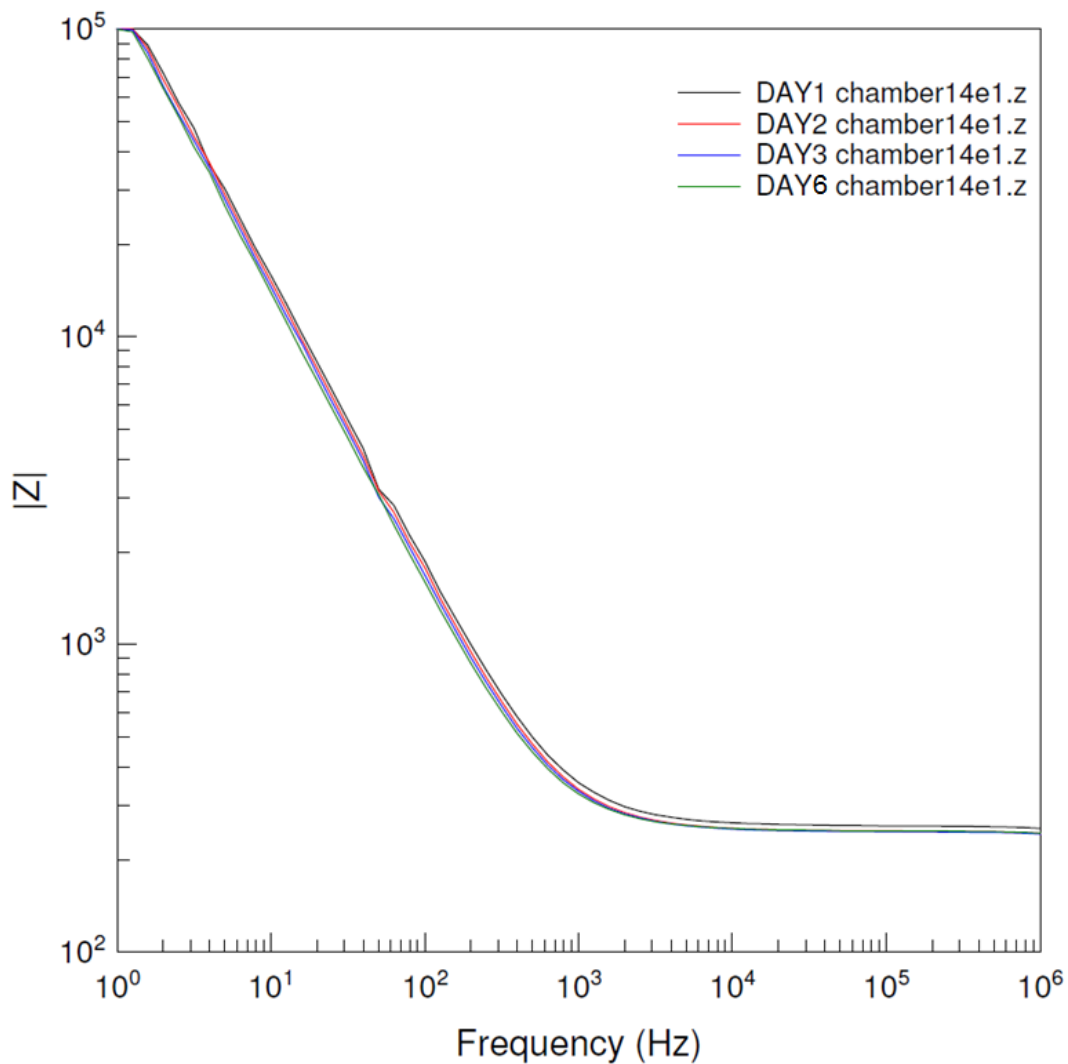
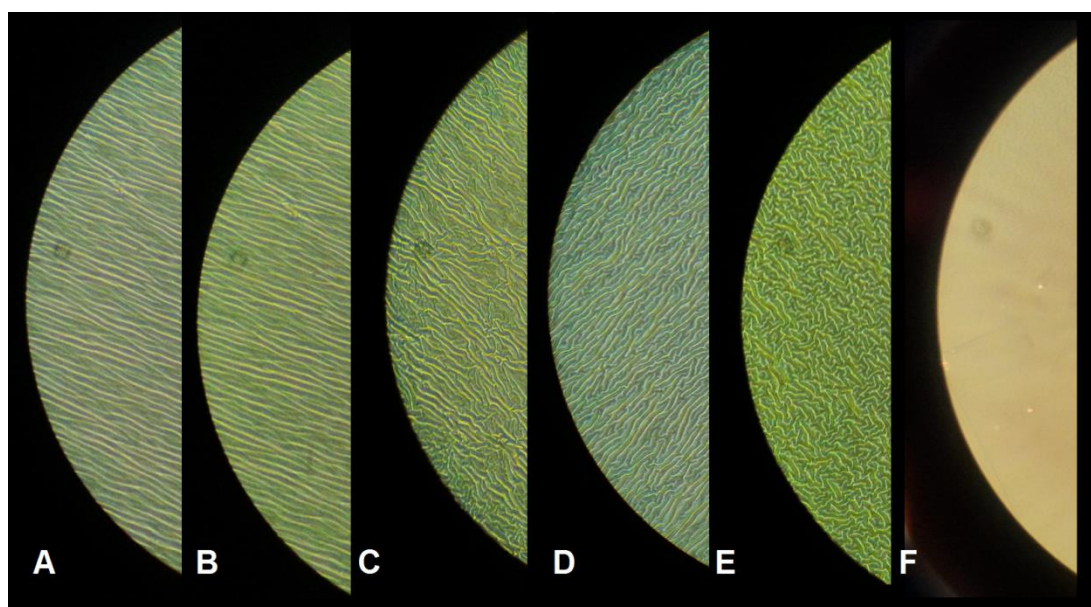


Figure 2.1: Complete graph of CH14E1 as an example of variability of  $|Z|$  impedance values measured in the total range of frequencies (0Hz to  $10^6$ Hz) across the 6 days with only medium as filled solution. The four impedance profiles seem very linear and parallel across the whole range of frequencies.

## Appendix B: Overheated substrates

If the dish is over heated during the sputter coating process (exposure to gold deposition is too long) special reliefs have been observed on the plastic substrate and seem to be dependent on the exposure time. This may be caused by the response of the plastic substrate to the heat generated during the sputter coating. Various styles of patterns have been observed ranging from simple mostly linear patterns (figure 2A) to highly complex organisations (figure 2F)

Figure 5.2 shows several examples taken via light microscopy with a magnification of x40.



**Figure 5.2: collection of samples of special reliefs observed on different places of the overheated substrate. The magnification is x 40. The images A-F shows different patterns observed on the same sample at different areas. The image F shows a normal flat gold layer, as used for the biosensor electrodes.**

This special relief may be interesting for cell adhesion characteristics as the relief of the cell substrate can dramatically change the cell shape and guidance (Peter Clark, 1994).

Those reliefs may have a utility in spatial organisation of the cells. If the cells proliferate inside those complex gold patterns, the impedance measures would be interesting to analyse as the cells may have a higher contact surface with the gold. This may also increase the interface surface between the cells and the gold.

## Appendix C: Future designs

The electrode used in this study is a macro-electrode and can monitor general cellular development and confluence of large population of cells. The magnitude of changes in the impedance has been shown to be dependent on the electrode surface covered by the cells and the surface roughness (Lind *et al.*, 1991).

Other studies (Sarró *et al.*, 2012; Abdur Rahman *et al.*, 2007; Wegener *et al.*, 2000) support that the degree of cell adherence on the electrode, the impedance of the measuring electrode alone, and the degree of cell confluence on the electrode have strong impact on accuracy and sensitivity of the system. In order to improve the existing system, several designs of possible masks have been designed as a side-development during this project. One of those designs is presented in figure 5.3.

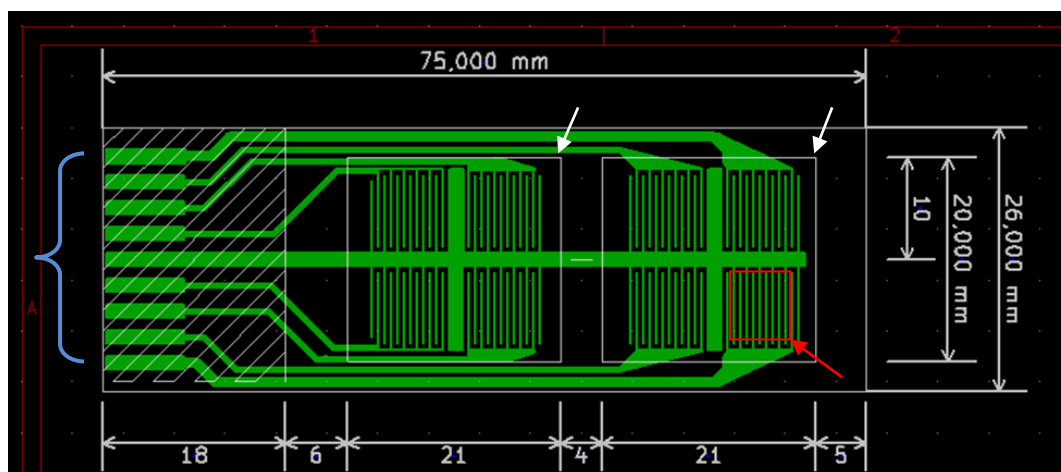


**Figure 5.3: Example of possible future design for biosensor masks: Inter-digital sensor array.** This mask aims to produce a gold electrode array to use as a substrate for the Labteckslide used in this study. The dimensions have been calculated to fit the proportions of the Labteck slide previously used (75 mm x 26mm), in order to be able to use the two culture cubes (White arrows) at the same time. This sensor is divided in 8 inter-digital micro zones. All the scales are in mm. Image designed with the open source software KiCad EDA Software Suite, 2014.

The inter-digital arrangement of the micro zones (red arrow shows one micro zone) draws gaps which are 380  $\mu\text{m}$  wide and are thought to considerably improve sensibility and precision. The left hand side (blue curly bracket) of the picture displays 9 connections that can be used to plug this micro device into a housing station.

The addition of the previous relief patterns (see Appendix B) and this type of electrode on figure 3 above may be interesting for future study.



## **6. Bibliography**

Abdur Rahman, A.R., Price, D.T., Bhansali, S., 2007. Effect of electrode geometry on the impedance evaluation of tissue and cell culture. *Sensors and Actuators B: Chemical*, Special Issue: Eurosensors XX The 20th European Conference on Solid-State Transducers the 20th European conference on Solid-State Transducers 127, 89–96.

Allen, T.D., Simmens, S.C., 1976. Conversion of vacuum coating units for sputter coating. *Micron* (1969) 7, 141–144

Beetner, D.G., Kapoor, S., Manjunath, S., Zhou, X., Stoecker, W.V., 2003. Differentiation among basal cell carcinoma, benign lesions, and normal skin using electric impedance. *IEEE Transactions on Biomedical Engineering* 50, 1020–1025

Benson, K., Cramer, S., Galla, H.-J., 2013. Impedance-based cell monitoring: barrier properties and beyond. *Fluids Barriers CNS* 10, 5.

Blaus, 2010. Creative common rights CC3.0 ,Blausen gallery 2014. *Wikiversity Journal of Medicine*.

Christopher McCormick. Studies on the development and assessment of a novel prostacyclin-eluting stent for the treatment of myocardial ischaemia. Thesis [Eng. D.] Department of Bioengineering University of Strathclyde, 2008.

Clark, P., Connolly, P., Curtis, A.S., Dow, J.A., Wilkinson, C.D., 1990. Topographical control of cell behaviour: II. Multiple grooved substrata. *Development* 108, 635–644.

Colombo, A., Drzewiecki, J., Banning, A., Grube, E., Hauptmann, K., Silber, S., Dudek, D., Fort, S., Schiele, F., Zmudka, K., Guagliumi, G., Russell, M.E., TAXUS II Study Group, 2003. Randomized study to assess the effectiveness of slow- and moderate-release polymer-based paclitaxel-eluting stents for coronary artery lesions. *Circulation* 108, 788–794.

Edouard Cheneau, Michael C. John, Jana Fournadjiev, Rosanna C. Chan, Han-Soo Kim, Laurent Leborgne, RajbabuPakala, Hamid Yazdi, Andrew E. Ajani, RenuVirmani, *et al.* *Circulation*. 2003 April 29; 107(16): 2153–2158.

Figure 1.2 & figure 1.3: American Heart Association, 2014,  
[http://watchlearnlive.heart.org/CVML\\_Player.php?moduleSelect=cstent](http://watchlearnlive.heart.org/CVML_Player.php?moduleSelect=cstent)

Flugelman, M.Y., Virmani, R., Leon, M.B., Bowman, R.L., Dichek, D.A., 1992. Genetically engineered endothelial cells remain adherent and viable after stent deployment and exposure to flow in vitro. *Circulation Research* 70, 348–354

Guo, S., DiPietro, L.A., 2010. Factors Affecting Wound Healing. *J Dent Res* 89, 219–229.

H. Martini, J.L. Nath, E.F. Bartholomew *Fundamentals of Anatomy & Physiology* (9th Edition), 2011

Jaffe, R., Strauss, B.H., 2007. Late and Very Late Thrombosis of Drug-Eluting Stents Evolving Concepts and Perspectives. *J Am CollCardiol* 50, 119–127

Jossinet, J., 1998. The impedivity of freshly excised human breast tissue. *PhysiolMeas* 19, 61–75.

Khandhar et Samuel, Electrical impedance spectroscopy measurements using a four-electrode configuration on Indian and Malaysian spicy dishes. *Biosensor Bioelectronics*, 2006 Feb;48(6):210-854.

Kipshidze, N., Dangas, G., Tsapenko, M., Moses, J., Leon, M.B., Kutryk, M., Serruys, P., 2004. Role of the endothelium in modulating neointimal formation: Vasculo-protective approaches to attenuate restenosis after percutaneous coronary interventions. *Journal of the American College of Cardiology* 44, 733–739.  
doi:10.1016/j.jacc.2004.04.048

Kirchengast, M., Münter, K., 1998. Endothelin and restenosis. *Cardiovascular Research* 39, 550–555

Knight, C.J., Curzen, N.P., Groves, P.H., Patel, D.J., Goodall, A.H., Wright, C., Clarke, D., Oldershaw, P.J., Fox, K.M., 1999. Stent implantation reduces restenosis in patients with suboptimal results following coronary angioplasty. *European Heart Journal*. 20, 1783–1790. doi:10.1053/euhj.1999.1545

Komatsu R, Ueda M, Naruko T, Kojima A, Becker AE. Neointimal tissue response at sites of coronary stenting in humans: macroscopic, histological, and immunohistochemical analyses. *Circulation* 1998;98:224–233

Lincoff, A.M., Popma, J.J., Ellis, S.G., Hacker, J.A., Topol, E.J., 1992. Abrupt vessel closure complicating coronary angioplasty: Clinical, angiographic and therapeutic profile. *Journal of the American College of Cardiology* 19, 926–935.

Lind, R., Connolly, P., Wilkinson, C.D.W., Breckenridge, L.J., Dow, J.A.T., 1991. Single cell mobility and adhesion monitoring using extracellular electrodes. *Biosensors and Bioelectronics* 6, 359–367

Lusis, A.J., 2000. Atherosclerosis. *Nature* 407, 233–241

Lvovich, V.F., 2012. Impedance Spectroscopy: Applications to Electrochemical and Dielectric Phenomena. John Wiley & Sons.

M. Y. Salame, S. Verheye, S. P. Mulkey, N. A. Chronos, S. B. King, 3rd, I. R. Crocker, K. A. Robinson The effect of endovascular irradiation on platelet recruitment at sites of balloon angioplasty in pig coronary arteries. *Circulation*. 2000 March 14; 101(10): 1087–1090.

Gopinath Mania, Marc D. Feldmanb, Devang Patelb, Mauli Agrawal. Coronary stents: A materials perspective. *Biomaterials* 28, 1689–1710

Matter CM1, Rozenberg I, Jaschko A, Greutert H, Kurz DJ, Wnendt S, Kuttler B, Joch H, Grünenfelder J, Zünd G, Tanner FC, Lüscher TF. Effects of tacrolimus or sirolimus on proliferation of vascular smooth muscle and endothelial cells. *Cardiovascular Pharmacology*. 2006 Dec; 48(6):286-92.

Mohan, S., Dhall, A., 2010. A comparative study of restenosis rates in bare metal and drug-eluting stents. *Int. J. Angiol.* 19, e66–72.

Mohr, F.W., Morice, M.-C., Kappetein, A.P., Feldman, T.E., Ståhle, E., Colombo, A., Mack, M.J., Holmes, D.R., Morel, M., Van Dyck, N., Houle, V.M., Dawkins, K.D., Serruys, P.W., 2013. Coronary artery bypass graft surgery versus percutaneous coronary intervention in patients with three-vessel disease and left main coronary disease: 5-year follow-up of the randomised, clinical SYNTAX trial. *Lancet* 381, 629–638

Muramatsu, T., Onuma, Y., Zhang, Y.-J., Bourantas, C.V., Kharlamov, A., Diletti, R., Farooq, V., Gogas, B.D., Garg, S., García-García, H.M., Ozaki, Y., Serruys, P.W., 2013. Progress in treatment by percutaneous coronary intervention: the stent of the future. *Revue Cardiology* 66, 483–496

NHS CHOICES/ report:

<http://www.nhs.uk/Conditions/Coronaryangioplasty/Pages/Introduction.aspx>

Ong, A.T.L., Aoki, J., Kutryk, M.J., Serruys, P.W., 2005. How to accelerate the endothelialization of stents. *Arch Mal Coeur Vaiss* 98, 123–126.

Pethig, R., Kell, D.B., 1987. The passive electrical properties of biological systems: their significance in physiology, biophysics and biotechnology. *Phys. Med. Biol.* 32, 933.

Rigaud B, Morucci JP, Chauveau N. Bioelectrical impedance techniques in medicine, 1996;24(4-6):257-351.

S.E Moulton, J.N Barisci, A Bath, R Stella, G.G Wallace, Studies of double layer capacitance and electron transfer at a gold electrode exposed to protein solutions, *Electrochimica Acta*, Volume 49, Issue 24, 30 September 2004, Pages 4223-4230

Sarró, E., Lecina, M., Fontova, A., Solà, C., Gòdia, F., Cairó, J.J., Bragós, R., 2012. Electrical impedance spectroscopy measurements using a four-electrode

configuration improve on-line monitoring of cell concentration in adherent animal cell cultures. *Biosensor Bioelectronics* 31, 257–263

Schwartz, R.S., Edwards, W.D., Bailey, K.R., Camrud, A.R., Jorgenson, M.A., Holmes, D.R., 1994. Differential neointimal response to coronary artery injury in pigs and dogs. Implications for restenosis models *Arteriosclerosis Thrombosis* 14, 395–400.

Serruys, P.W., de Jaegere, P., Kiemeneij, F., Macaya, C., Rutsch, W., Heyndrickx, G., Emanuelsson, H., Marco, J., Legrand, V., Materne, P., 1994. A comparison of balloon-expandable-stent implantation with balloon angioplasty in patients with coronary artery disease. Benestent Study Group. *N. Engl. J. Med.* 331, 489–495.

Shedden, L., Kennedy, S., Wadsworth, R., Connolly, P., 2010. Towards a self-reporting coronary artery stent measuring neointimal growth associated with in-stent restenosis using electrical impedance techniques. *Biosensor Bioelectronics*.

Shedden Laurie, The intelligent stent, University of Strathclyde, 2008, Thesis (Ph.D.)

Sigwart, U., Puel, J., Mirkovitch, V., Joffre, F., Kappenberger, L., 1987. Intravascular stents to prevent occlusion and restenosis after transluminal angioplasty. *N. Engl. J. Med.* 316, 701–706

Stolwijk, J.A., Michaelis, S., Wegener, J., 2012. Cell Growth and Cell Death Studied by Electric Cell-Substrate Impedance Sensing, in: Jiang, W.G. (Ed.), *Electric Cell-Substrate Impedance Sensing and Cancer Metastasis*, Cancer Metastasis - Biology and Treatment. *Springer Netherlands*, P96

Stone, G.W., Parise, H., Witzenbichler, B., Kirtane, A., Guagliumi, G., Peruga, J.Z., Brodie, B.R., Dudek, D., Möckel, M., Lansky, A.J., Mehran, R., 2010. Selection Criteria for Drug-Eluting Versus Bare-Metal Stents and the Impact of Routine Angiographic Follow-Up: 2-Year Insights From the HORIZONS-AMI

(Harmonizing Outcomes With Revascularization and Stents in Acute Myocardial Infarction) Trial. *Journal of the American College of Cardiology* 56, 1597–1604.

Sumpio, B.E., Riley, J.T., Dardik, A., 2002. Cells in focus: endothelial cell. *Int. J. Biochem. Cell Biol.* 34, 1508–1512.

Süselbeck, T., Thielecke, H., Weinschenk, I., Reininger-Mack, A., Stieglitz, T., Metz, J., Borggrefe, M., Robitzki, A., Haase, K.K., 2005. *In vivo* intravascular electric impedance spectroscopy using a new catheter with integrated microelectrodes. *Basic Res. Cardiol.* 100, 28–34.

Tanous, D., Bräsen, J.H., Choy, K., Wu, B.J., Kathir, K., Lau, A., Celermajer, D.S., Stocker, R., 2006. Probucol inhibits in-stent thrombosis and neointimal hyperplasia by promoting re-endothelialization. *Atherosclerosis* 189, 342–349.

Valentinuzzi, M.E., Morucci, J.P., Felice, C.J., 1996. Bioelectrical impedance techniques in medicine. Part II: Monitoring of physiological events by impedance. *Crit Rev Biomed Eng* 24, 353–466.

Valgimigli, Marco Borghesi, Matteo Tebaldi, Pascal Vranckx, Giovanni Parrinello, Roberto Ferrari, *Eur Heart J.* 2013;34(12):909-919. A Pre-Specified Analysis From the Prolonging Dual Antiplatelet Treatment After Grading Stent-Induced Intimal Hyperplasia Study (PRODIGY)

Vodovotz Y, Waksman R, Kim WH, *et al.* Effect of coronary radiation on thrombosis following balloon overstretch injury in the porcine model. *Circulation.* 1999;100:2527–2533

Watt, J., Kennedy, S., McCormick, C., Agbani, E.O., McPhaden, A., Mullen, A., Czudaj, P., Behnisch, B., Wadsworth, R.M., Oldroyd, K.G., 2013. Succinobucol-Eluting Stents Increase Neointimal Thickening and Peri-Strut Inflammation in a Porcine Coronary Model. *Catheter Cardiovasc Interv* 81, 698–708

Wegener, J., Keese, C.R., Giaever, I., 2000. Electric Cell–Substrate Impedance Sensing (ECIS) as a Noninvasive Means to Monitor the Kinetics of Cell Spreading to Artificial Surfaces. *Experimental Cell Research* 259, 158–166

Wegener, J., Sieber, M., Galla, H.J., 1996. Impedance analysis of epithelial and endothelial cell monolayers cultured on gold surfaces. *J. Biochem. Biophys. Methods* 32, 151–170.

Wessely, R., Schömig, A., Kastrati, A., 2006. Sirolimus and Paclitaxel on Polymer-Based Drug-Eluting Stents: Similar But Different. *Journal of the American College of Cardiology* 47, 708–714

Wiskirchen J, Schober W, Schart N, *et al.* The effects of paclitaxel on the three phases of restenosis: smooth muscle cell proliferation, migration, and matrix formation: an in vitro study. *Invest Radiol* 2004;39:565–71

Xiao, C., Luong, J.H.T., 2003. On-Line Monitoring of Cell Growth and Cytotoxicity Using Electric Cell-Substrate Impedance Sensing (ECIS). *Biotechnol Progress* 19, 1000–1005.

Zhao, N., Watson, N., Xu, Z., Chen, Y., Waterman, J., Sankar, J., Zhu, D., 2014. In Vitro Biocompatibility and Endothelialisation of Novel Magnesium-Rare Earth Alloys for Improved Stent Applications

Zhong, Q., Mao, Q., Yan, J., Liu, W., Zhang, T., Liu, J., 2014. Real-time in situ monitoring of poly(lactide-co-glycolide) coating of coronary stents using electrochemical impedance spectroscopy. *J. Biomed. Mater. Res. Part B Appl. Biomater.*

Zou, Y., Guo, Z., 2003. A review of electrical impedance techniques for breast cancer detection. *Med EngPhys* 25, 79–90.



---

*Perfer et obdura; dolor hic tibi proderit olim.*